

# CEBAF Program Advisory Committee Six (PAC6) Proposal Cover Sheet

This proposal must be received by close of business on April 5, 1993 at:

CEBAF  
User Liaison Office  
12000 Jefferson Avenue  
Newport News, VA 23606

## Proposal Title

"Applications of Channeling Radiation"

## Contact Person

**Name:** P.W. Marshall  
**Institution:** SFA, Inc.  
**Address:** 1401 McCormick Drive  
**Address:**  
**City, State ZIP/Country:** Landover, MD 20785  
**Phone:** (301) 925-9400 **FAX:** (301) 925-8612  
**E-Mail → BITnet:** **Internet:**

If this proposal is based on a previously submitted proposal or letter-of-intent, give the number, title and date:

## CEBAF Use Only

Receipt Date: 4/5/93 Log Number Assigned: PR 93-045

By: SP

# **Applications of Channeling Radiation**

**B.L. Berman\*†§**

Department of Physics, The George Washington University  
Washington, DC 20052

**P.W. Marshall\*‡§** and **B.J. Faraday§**

SFA, Inc., 1401 McCormick Drive  
Landover, MD 20785

**H. Überall§**

Department of Physics, Catholic University of America  
Washington, DC 20064

**X.K. Maruyama§**

Department of Physics, U.S. Naval Postgraduate School  
Monterey, CA 93943

**W.J. Beezhold**

Radiation Effects Division, Sandia National Laboratories  
Albuquerque, NM 87185

**G.R. Neil**

Accelerator Division, CEBAF  
Newport News, VA 23606

\* Co-Spokesperson

† Will present proposal

‡ Contact person

§ For the purpose of developing channeling radiation applications, these individuals are representing SFA, Inc. with support through the Department of Energy SBIR contract number DE-FG05-90-ER81034.

## 1. PROPOSAL AND MOTIVATION

We propose to test the feasibility of using channeling radiation as the source of radiation for microlithography. Channeling radiation is very intense, forward-directed, easily tunable, narrow-band radiation that is produced when an electron beam is directed along a major axis or plane in a single crystal. Because of these properties and especially because channeling radiation of a few keV (in the x-ray region) can be produced by electrons of only a few MeV, many important applications may be feasible. Among these are microlithography, angiography, molecular-structure analysis by x-ray diffraction, and elemental analysis by x-ray fluorescence. Since high-intensity electron accelerators of only a few MeV are inexpensive (relative to GeV synchrotrons, for example), and since electron accelerators with the very low emittance necessary for most of the electrons to be channeled in a crystal target now have been shown to be practical, widespread use of this kind of radiation source might be envisioned.

SFA, Inc. has proposed to test the feasibility of these possible applications of channeling radiation, and has been awarded a Phase II SBIR grant by the DOE to do so. After studying the electron beam properties at a conventional linac (at AFRRI, in Bethesda, MD), we concluded that such applications were best accomplished only with one of the new generation of low-emittance accelerators. The CEBAF injector is the best electron accelerator in the world in this energy range, it is in the United States so that we have control over technology-transfer issues, it is a DOE facility, and it is conveniently located for us so that we can make measurements here on short notice and hence with very little disruption of the CEBAF construction or operations schedule. Therefore, we propose to set up a beam line for producing channeling radiation at the 5-MeV stage of the CEBAF injector, and to carry out feasibility studies of applications of channeling radiation, the first of which would be for the lithography of silicon wafers on a submicron scale.

## 2. INTRODUCTION TO AND HISTORY OF CHANNELING RADIATION

When a relativistic charged particle passes through a single crystal very nearly parallel to a major crystalline plane or axis so that it is channeled in that direction, it undergoes periodic motion in the plane transverse to this direction, and hence it can radiate. Quantum mechanically, this channeling radiation corresponds to a radiative transition between two eigenstates of the transverse crystalline potential; when the transition occurs between two bound states, a sharp spectral line is emitted. When there are only two bound states (for incident electrons), or when the interplanar potential is nearly harmonic (as it is for incident positrons), the emitted radiation is nearly monochromatic. In the forward direction in the laboratory frame of reference, the radiation is transformed upwards in energy. In part, this is because of the relativistic velocity of the charged particle that leads to a factor of  $\gamma = E/mc^2$ , where  $E$  is the total energy of the particle and  $m$  is its rest mass (this can also be thought of as a deepening of the crystalline potential well by a factor of  $\gamma$ ). The Doppler shift gives rise to an additional factor of  $2\gamma$  in the forward direction. This combined factor of  $2\gamma^2$  (equal to 200 for  $\gamma=10$ , corresponding to electrons or positrons of about 5 MeV, for example) brings the channeling radiation up into the interesting and useful keV energy region, and also makes it relatively easy to observe, using the well known methods of x-ray spectroscopy. This large lever arm also makes it easy to tune channeling radiation, by varying the incident particle energy over a relatively narrow range. The same relativistic transformation folds the radiation forward in the laboratory into a narrow cone having a characteristic half-angle of  $1/\gamma$  (equal to about 6 deg in the above example), and thus makes it very intense within that solid angle. For the case of planar channeling, the radiation is linearly polarized. [One notes in passing that for electron energies of a few GeV, the laboratory energies of channeling radiation lie in the range of a few tens of MeV, and since the intensities (see below) are about 4-5 orders of magnitude greater than the most intense tagged photon beam, there might very well be important and heretofore unthought-of photonuclear experiments that can be done at CEBAF.]

In the approximation that the field source of the transverse crystalline potential can be represented by planar sheets or axial strings of charge, the particle-crystal system is equivalent to a one- or two-dimensional hydrogenic atom (for the planar and axial cases, respectively). This establishes selection rules for the radiative transitions, and enables one to predict many of the detailed properties of channeling radiation by analogy with these simple quantum-mechanical systems. In fact, the theory of channeling radiation (see below) has progressed far beyond these simple considerations, and detailed predictions of channeling-radiation spectral energies, widths, and intensities now are made routinely with the use of many-beam (i.e., many Fourier-component) calculations using wave functions deduced from electron-scattering form factors (for the atoms in the crystal) which also reflect the periodicity of the crystalline potential. Also included in modern calculations are the effects of multiple scattering, dechanneling, bremsstrahlung production, and crystal lattice vibrations.

Channeling radiation was first observed at the Lawrence Livermore Laboratory in 1968 as a low-energy enhancement in the forward radiation spectrum from 16- and 28-MeV positrons and electrons axially channeled in a silicon crystal.<sup>1</sup> Theoretical predictions by Kumakhov and by Terhune and Pantell in the mid-seventies<sup>2</sup> inspired further investigations at Livermore and elsewhere, and the first observations of spectral peaks, for both axial and planar channeling radiation, from 56-MeV positrons and electrons, were made in 1978.<sup>3</sup> The first observation of sharp spectral lines, shown in Fig. 1, was made possible by very tight collimation together with the use of a diamond crystal, at Saclay in late 1980.<sup>4</sup> Meanwhile, channeling-radiation studies at higher energies (in the GeV region) were carried out at Tomsk, Yerevan, SLAC, Kharkov, Serpukhov, and CERN,<sup>5</sup> and at lower energies (a few MeV) at Albany, Illinois, and especially Aarhus.<sup>6</sup> Subsequent measurements at several of these laboratories, especially at Livermore,<sup>7</sup> have resulted in the development of a rich literature on the subject in just a few years. The subjects studied, in addition to the characteristics of the channeling radiation itself, include (a) properties of perfect crystals, such as high-resolution (of the order of 0.1 Å) mapping of the interplanar and interstring potentials, determination of Debye temperatures (to about 10 K) and thermal vibration amplitudes (to about  $10^{-3}$  Å) along each major crystalline direction, and occupation lengths (to about 1 or 2 μm) of channeled positrons and electrons; (b) defects and impurities in imperfect crystals, such as the location and extent of platelets in diamond along each of the three major crystalline directions; and (c) factors facilitating or limiting the use of channeling radiation as a photon source, such as radiation damage in both silicon and alkali-halide crystals and the dependence of radiation intensity on crystal species and thickness. A recent monograph by Kumakhov and Wedell<sup>8</sup> constitutes a comprehensive review of all but the most recent literature, both theory and experiment. Very recently, the first results from the channeling-radiation facility at the new Darmstadt superconducting linac have been published,<sup>9</sup> which show that the intensity of channeling radiation (but not necessarily its spectral shape) scales linearly with electron beam current, at least up to 60 μA. This last result certainly augurs well for the feasibility of channeling radiation as an intense radiation source for applications.

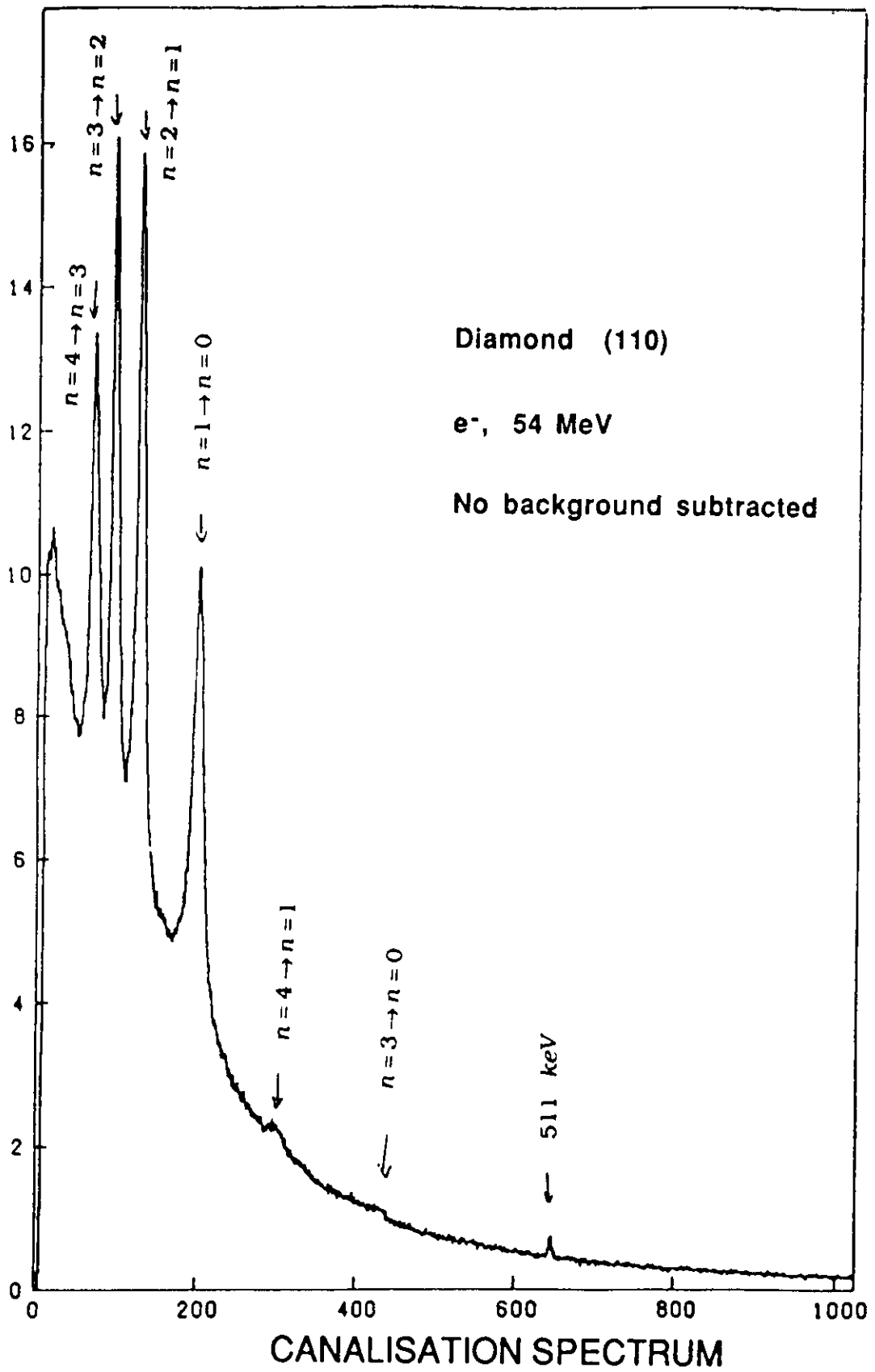


Figure 1:

First channeling-radiation spectrum from diamond.

### 3. REPRESENTATIVE EXAMPLES OF CHANNELING-RADIATION SPECTRA

We give here several representative examples of planar and axial channeling-radiation spectra, for electrons incident on silicon and diamond crystals. These spectra are the ones in the literature that most closely approximate the cases of interest for our proposed applications. Electrons are chosen because of obvious intensity considerations--positron beams are at least three orders of magnitude weaker. Silicon and diamond crystals are chosen for at least six reasons: (a) the literature contains many examples (especially for silicon); (b) perfect or nearly perfect crystals (especially silicon) are available; (c) they have the same crystal structure, which facilitates comparisons; (d) they (especially diamond) have relatively low atomic number, so that the spacing between energy levels is relatively large, and hence conditions can be found where there are only two bound states and therefore only a single spectral line will be emitted; (e) they (especially diamond) have high Debye temperatures, so that the spectral lines will be narrow; and (f) they, unlike alkali halides, for example, have been shown (silicon) or calculated (diamond) to be least susceptible to radiation damage.

Crystals with high atomic number, such as tungsten, should yield higher intensity channeling radiation, for lower energy electron beams, because of their deeper crystalline potentials, but at the cost of the loss of monochromaticity because of the multiplicity of bound states and the subsequent much wider bandwidth. Still, such crystals will be part of our experimental program because at least one of our listed applications, namely microlithography, is not critically dependent on a narrow-bandwidth source. However, no examples for low-energy incident electrons appear in the literature--only a single spectrum, for 54-MeV electrons, has been obtained (at Livermore<sup>10</sup>).

Figure 2 shows planar channeling-radiation potentials and spectra from the three major planes in diamond for incident electrons of 12.6 MeV.<sup>11</sup> For the (100) plane, the  $n=1$  level is barely bound, so that the channeling-radiation peak corresponding to the  $1 \rightarrow 0$  transition is broad and hence poorly defined. For the (110) plane, the  $1 \rightarrow 0$  peak is sharp and higher in energy, and the  $2 \rightarrow 1$  peak is broad, corresponding to the  $n=2$  level being barely bound. For the double-well (111) plane (see below), the  $2 \rightarrow 1$  and  $3 \rightarrow 2$  peaks are clearly seen, but the  $1 \rightarrow 0$ ,  $4 \rightarrow 3$ , and  $5 \rightarrow 4$  peaks lie lower in energy than the detector threshold.

Figures 3 and 4 show axial channeling-radiation potentials and spectra from two major axes in diamond--Fig. 3 for 4-MeV electrons incident along the  $\langle 110 \rangle$  axis<sup>12</sup> and Fig. 4 for 12.6-MeV electrons incident along the  $\langle 100 \rangle$ ,  $\langle 110 \rangle$ , and  $\langle 112 \rangle$  axes.<sup>11</sup> Since axial potentials are two-dimensional instead of one-dimensional, the labeling of the energy levels follows the notation of atomic physics, and when two atomic planes or rows in a crystal lie in close proximity, as in the case of the (111) or  $\langle 110 \rangle$  directions in diamond, the potentials from these planes or rows overlap, forming a saddle point. For the axial case shown in Fig. 3, obtained at the lower electron energy, the  $2p$  states lie above the saddle point and split into four molecular-type levels; the splitting of the  $2p \rightarrow 1s$  transitions here can be seen clearly. The calculated curves assume equal populations and

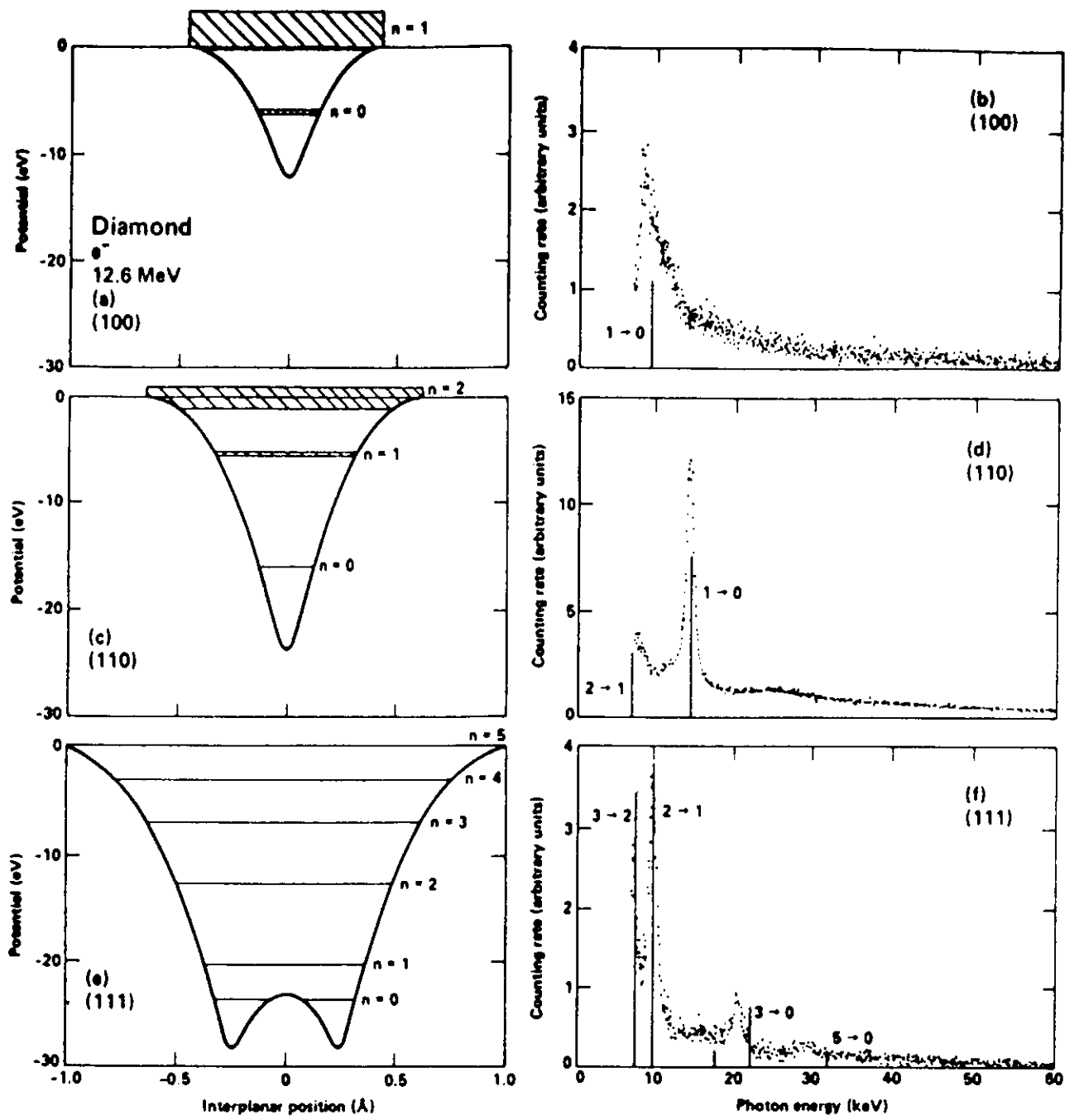


Figure 2:

Planar channeling-radiation spectra for 12.6-MeV electrons in diamond.

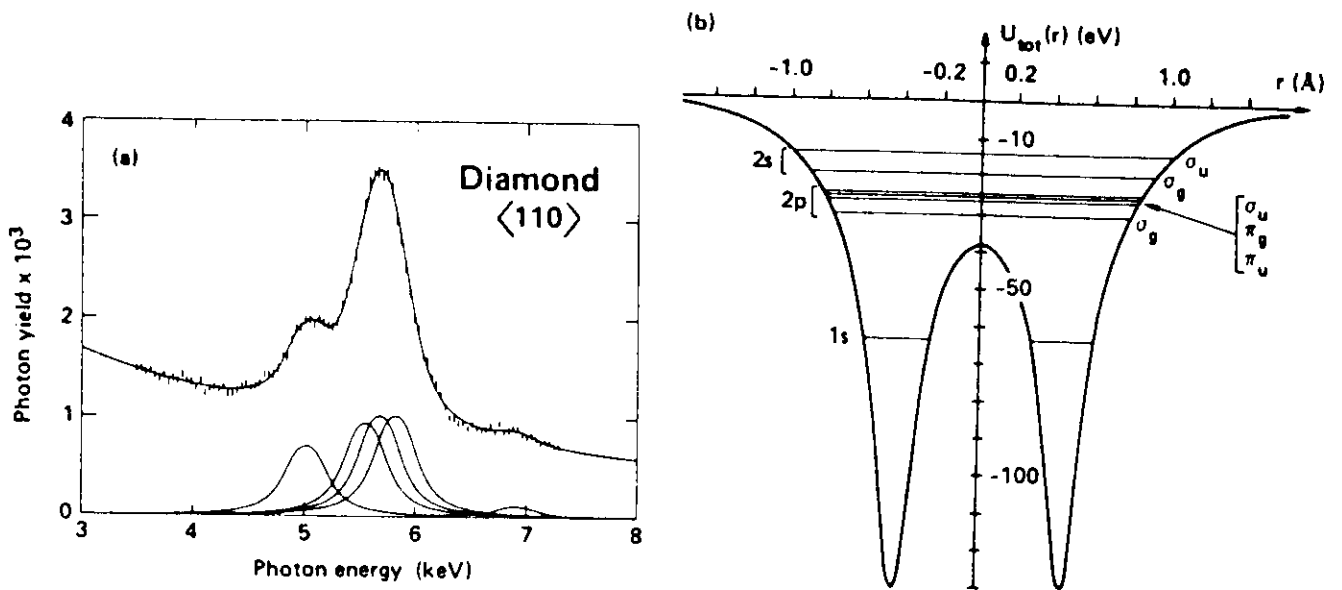


Figure 3:

For 4-MeV electrons channeled along the  $\langle 110 \rangle$  axial direction in diamond: (a) measured photon spectrum and (b) calculated potential and energy levels. The fitting of the  $2p \rightarrow 1s$  lines in (a) involves assumptions of equal populations of the  $2p$  levels, which is expected because of incoherent scattering, and of equal widths, which is anticipated because of the dominance of the  $1s$  state in the determination of the coherence lengths.

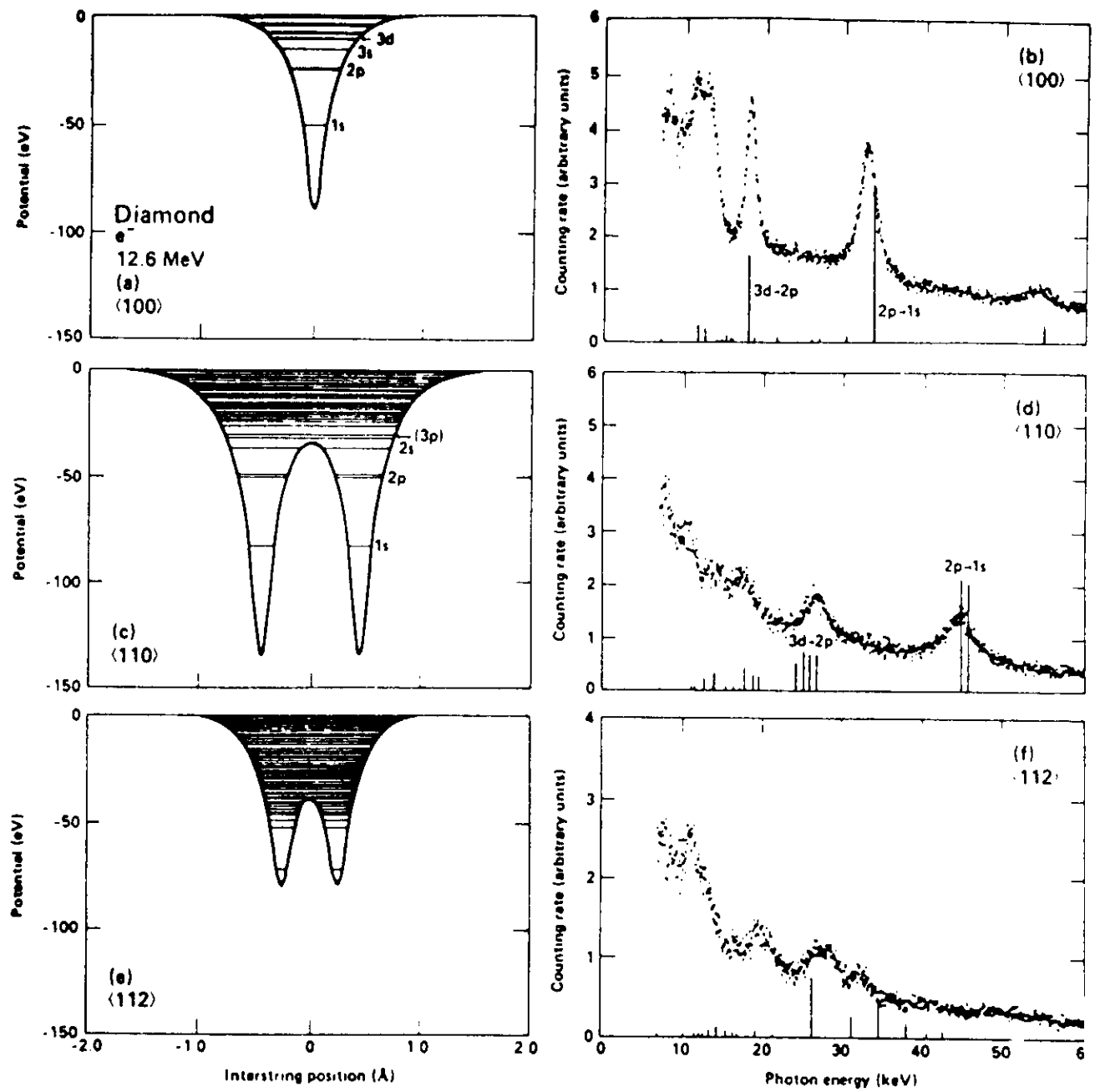


Figure 4:

Axial channeling-radiation spectra for 12.6-MeV electrons in diamond.

equal widths, both very good assumptions for this case. In Fig. 4, for the  $\langle 100 \rangle$  axis the  $3d \rightarrow 2p$  peak is seen to be even sharper than that for the (unresolved)  $2p \rightarrow 1s$  peak, while for the  $\langle 110 \rangle$  and  $\langle 112 \rangle$  axes the proliferation of energy levels is seen to result in more complex spectral structure.

Figure 5 shows the potentials and Fig. 6 the radiation spectra for electrons of 4 different energies incident along the (100) plane of silicon.<sup>13</sup> One sees the number of bound levels and hence the number of bound-to-bound transitions increase with energy. The calculated curves in Fig. 6 take into account the major line-broadening effects, such as multiple scattering and thermal vibrations.

Figure 7 shows the radiation spectrum for 3.5-MeV electrons channeled along the  $\langle 111 \rangle$  axis of silicon, cooled to 110 K.<sup>14</sup> Comparison with Fig. 3 shows that the higher atomic number of silicon deepens the potential and binds more energy levels than that of diamond; here, in addition to the  $2p \rightarrow 1s$  transitions, the  $3d \rightarrow 2p$  and even the  $3p \rightarrow 1s$  transitions are present.

These representative results from the literature indicate a number of the ways one can achieve channeling-radiation spectra in the photon energy range and perhaps monochromaticity of interest for a given application. In other words, they, together with other previous results, provide us with a road map so that we can test the feasibility of producing a useful radiation source with a minimum of unnecessary searching for the best crystal parameters and experimental running conditions.

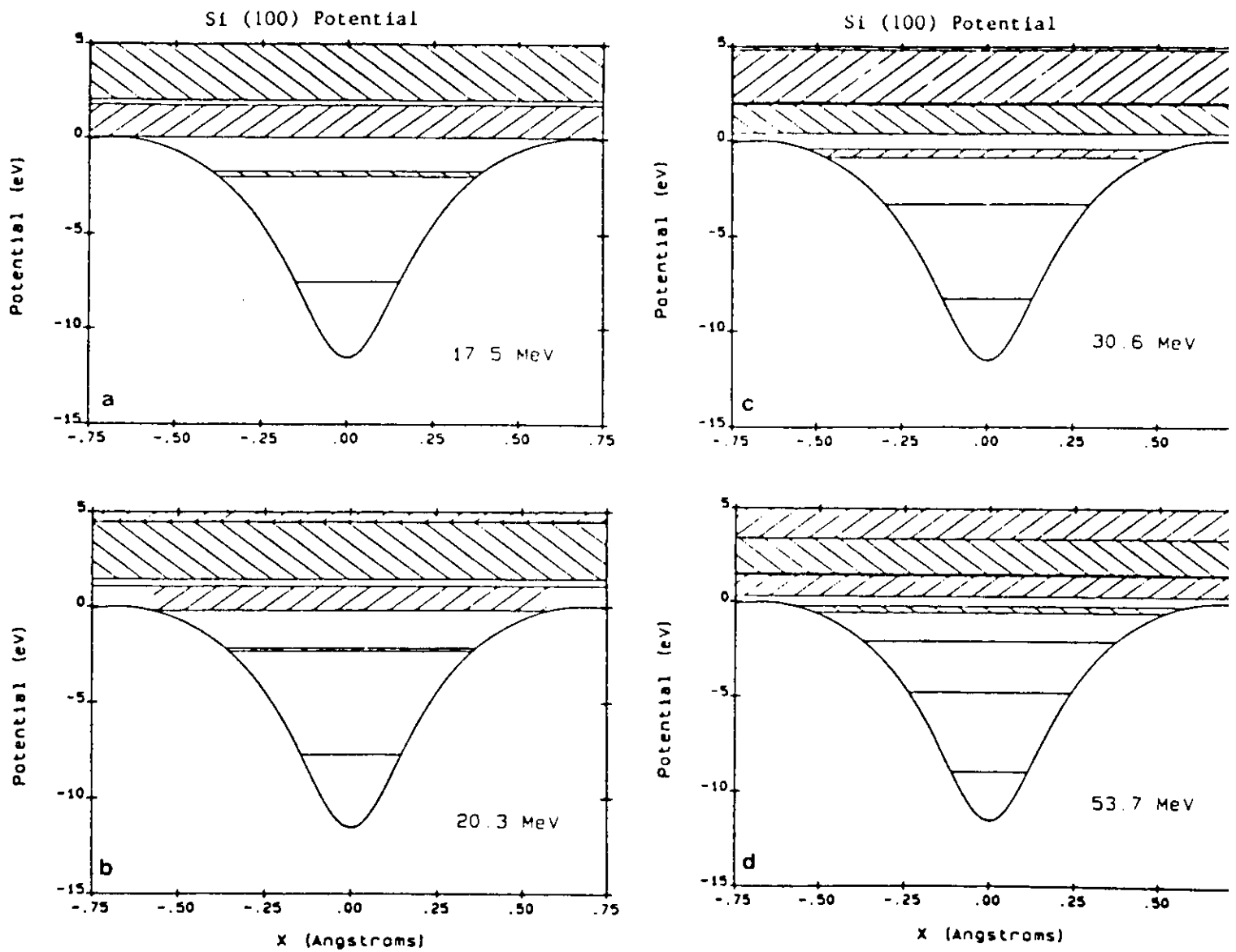


Figure 5:

Calculated interplanar potentials and energy levels for electrons channeled along the (100) planes of silicon, having energies of (a) 17.5 MeV, (b) 20.3 MeV, (c) 30.6 MeV, and (d) 53.7 MeV.

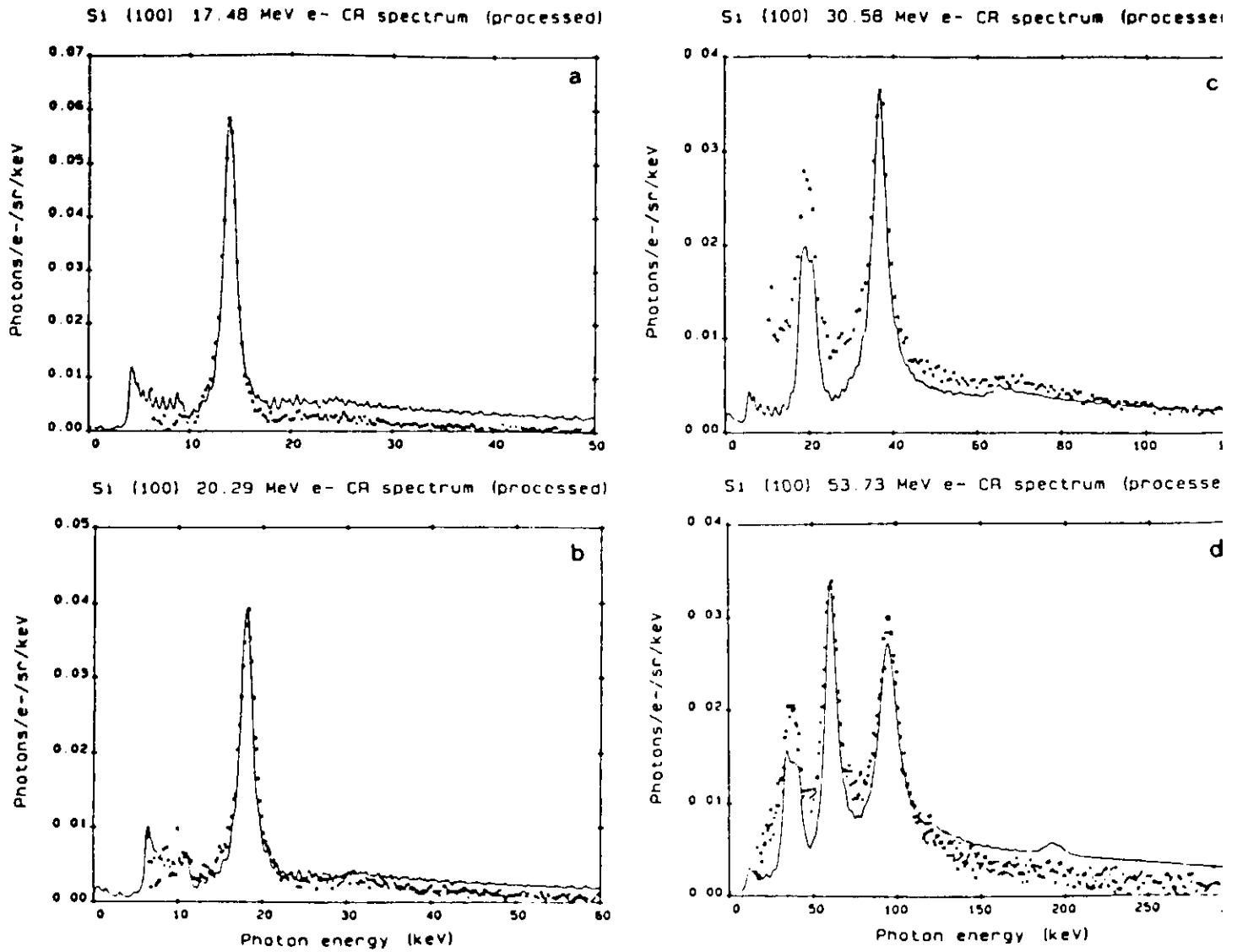


Figure 6:

Radiation spectra from electrons channeled along the (100) planes of silicon, having energies of (a) 17.5 MeV, (b) 20.3 MeV, (c) 30.6 MeV, and (d) 53.7 MeV. The curves fitted to the data are the results of many-beam calculations.

Si <111>

3.5 MeV e<sup>-</sup>

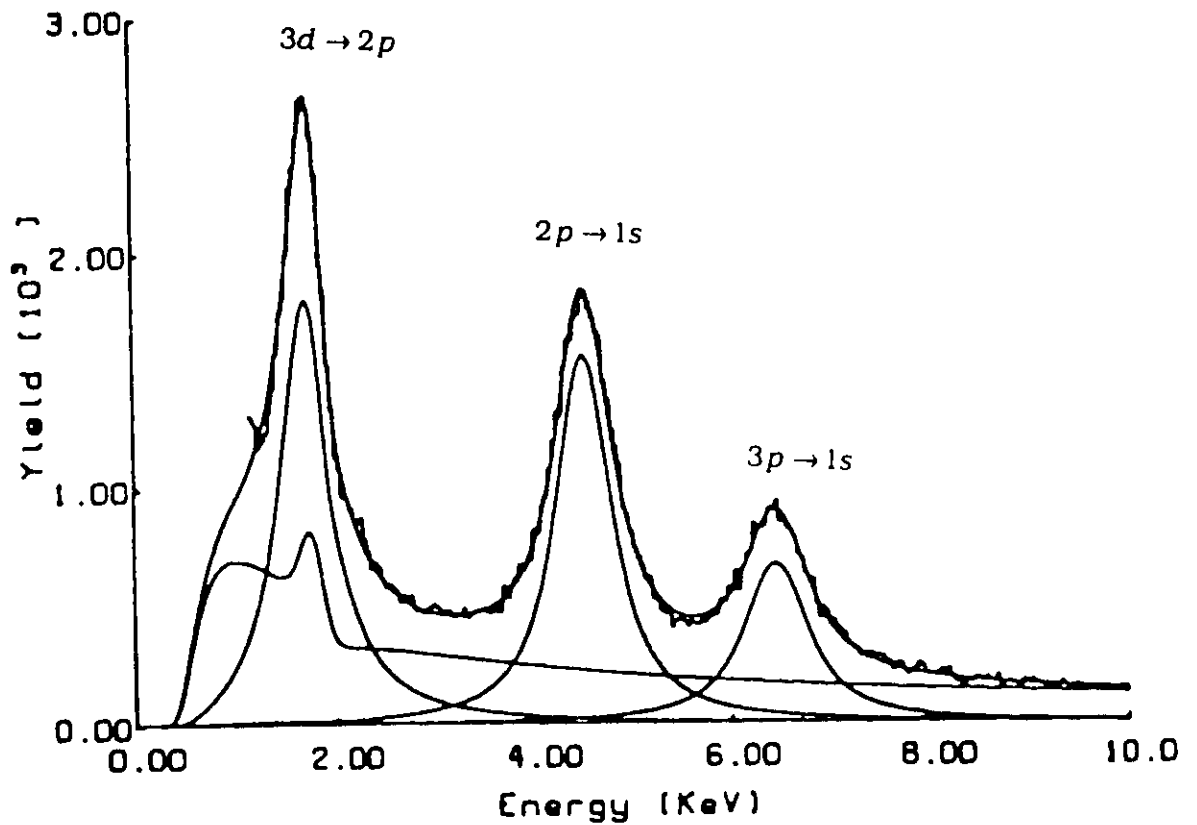


Figure 7:

Experimental photon spectrum (histogram) for 3.5-MeV electrons on a 0.5- $\mu$ m Si crystal  $0.1^\circ$  from a <111> axis. The smooth curves show the fit and its components, an intensity-scaled background and three channeling-radiation lines, the 3d  $\rightarrow$  2p, the 2p  $\rightarrow$  1s, and the 3p  $\rightarrow$  1s transitions.

#### 4. THEORY OF CHANNELING RADIATION

When relativistic electrons, whether of energies in the MeV region or up into the GeV region, traverse a crystal target, interference effects due to the regular spacing of the lattice atoms modify drastically the radiation which they would normally emit in the form of (incoherent) bremsstrahlung (IB) upon traversal of an amorphous target. The electron trajectory (a) in Fig. 8 instead gives rise to coherent bremsstrahlung (CB).<sup>15</sup> If the angle of incidence made by the electron with a lattice plane,  $\theta$ , falls below the Lindhard critical angle,  $\theta_L = (Ze^2/Ed)^{1/2}$ , where  $E$  is the total electron energy and  $d$  the spacing of the lattice planes, then the Coulomb force of the plane (which in the Lindhard approximation may be considered as continuous) traps the electron as in Fig. 8, trajectory (b). The ensuing radiation is known as channeling radiation (CR).<sup>3,16,17</sup>

Both of these types of coherent radiation are characterized by spectral lines that are quasimonochromatic, nearly 100% linearly polarized, and tunable. Figure 9 shows qualitatively the appearance of these lines. There are two kinds of CB, called type B (Fig. 9a), with lines located at photon energies  $k \cong 0.1E$  and up, and type A (Fig. 9b), with lines at  $k \cong 0.01E$  and up (they disappear at  $\theta = 0$ ) and of an intensity  $\sim 10$  times that of the type B lines. Finally, the CR lines (Fig. 9c) are located at  $k \cong 0.001E$  and are again more intense than the CB, type A lines. CR corresponding to Fig. 8 is called planar CR.

There also exists the possibility that the electrons can get trapped by a crystal axis (which in the Lindhard approximation is treated as a continuous string of charge), carrying out a "rosette motion" while propagating along the axis. The radiation they emit is called axial CR; it also is emitted in the form of spectral lines, which are more densely spaced and more intense than in planar CR.

The lines in Fig. 9 were calculated taking all photon emission directions  $\theta$  into account. The emission is largely forward ( $\theta$  is characteristically  $1/\gamma = m/E$ ,  $m$  being the electron mass); if the photon counter has an opening angle smaller than  $1/\gamma$ , the width of the lines in Fig. 9 will be limited further by a lower cutoff. The thermal motion of the lattice atoms will reduce the intensities of CB and CR,<sup>15</sup> generating at the same time a smooth IB background that varies as  $1/k$ , with the (now reduced) CB and CR lines superimposed on the background.

An overview of typical CR spectra, observed at various energies and using different crystal targets, has been given above. This overview also includes some results of theoretical calculations of CR peak positions in energy, their intensities, and their widths. The theory of peak positions and intensities is based on the use of Bloch functions for the electrons in a periodic lattice, but since Lindhard's continuum approximation for crystal planes or for crystal axes can be adapted to a very good approximation for relativistic electrons,<sup>18</sup> these Bloch functions are one-dimensional or two-dimensional, respectively (as are the associated Brillouin zones). We have written both planar and axial many-beam codes for the Bloch functions and the transverse crystal potentials which

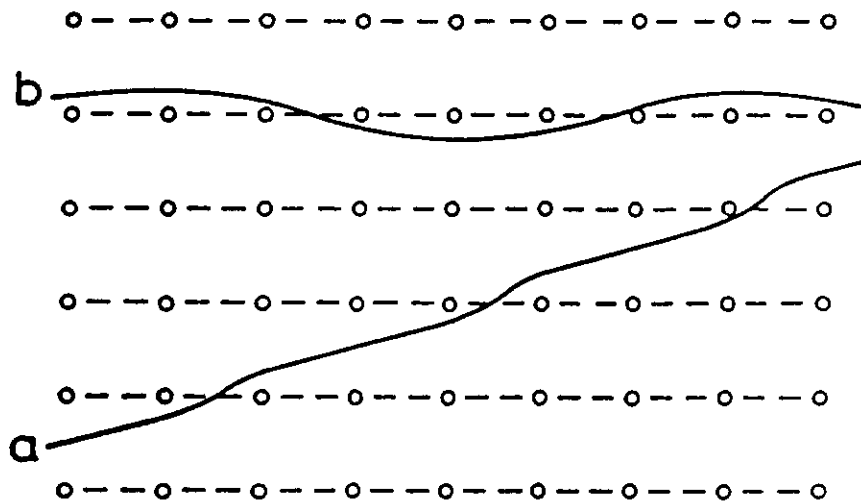


Figure 8:

Qualitative illustration of classical electron motion, governed in effect by a continuum planar potential. The angles of the paths to the crystal planes are greatly exaggerated.

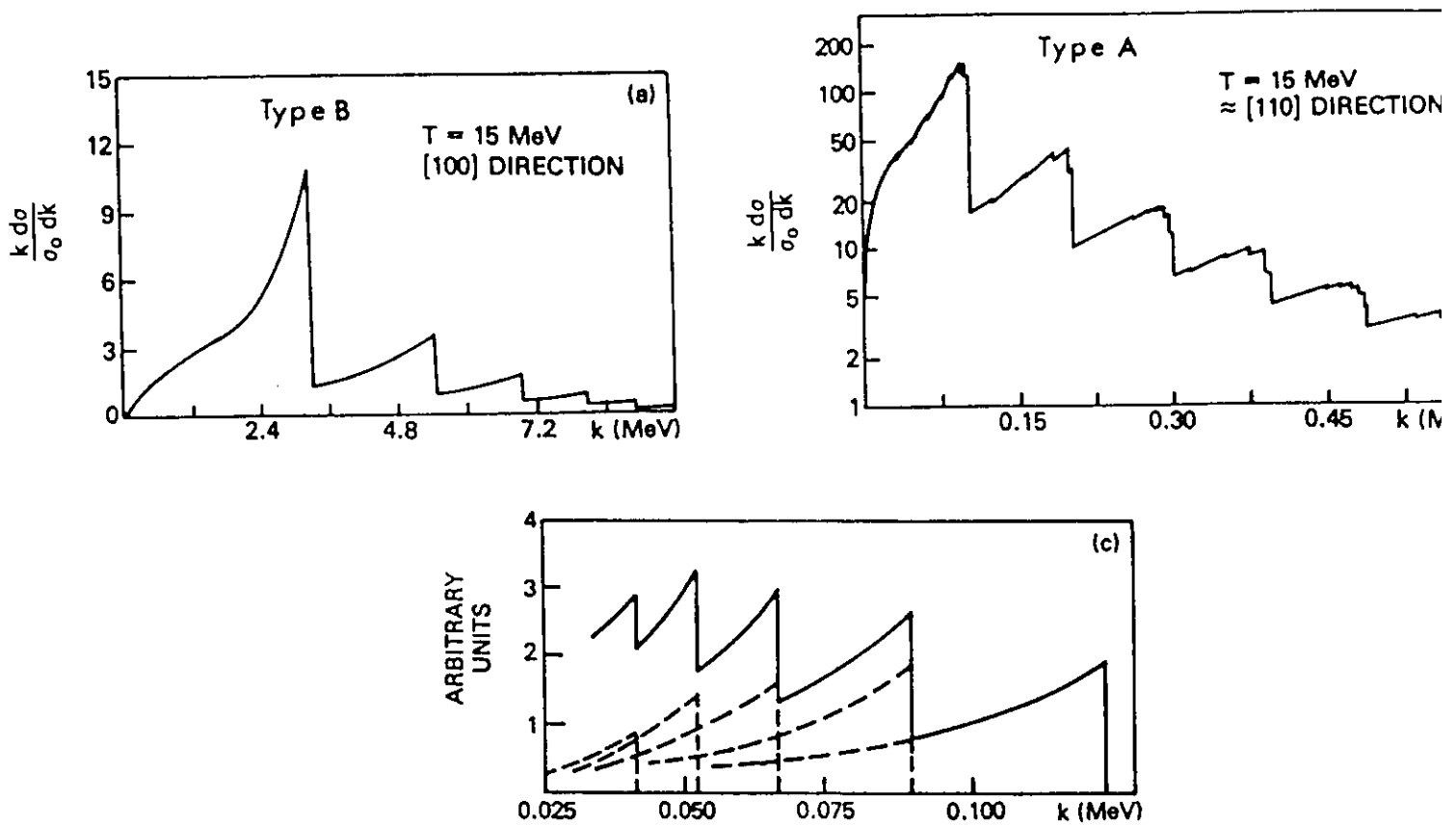


Figure 9:

Peaks in the spectrum of coherent bremsstrahlung, (a) of type B and (b) of type A, from 15-MeV electrons, and in the spectrum of channeling radiation (c) from 56-MeV electrons, all in a silicon crystal target.

reproduce exactly the earlier results found in the literature, and which in addition obtain unbound states, which had not been done previously for axial channeling.

The procedure for obtaining one-dimensional Bloch functions has been outlined by Andersen *et al.*<sup>19</sup> and will be discussed here only briefly. If  $x$  is the direction transverse to a continuum plane, and the projection of the electron momentum on that plane is taken as the  $z$  direction, the Bloch wave function of the channeled electron is

$$\psi_{\mathbf{k}}(\mathbf{r}) = e^{i\mathbf{k}z} u(x, t); \quad (1)$$

here,  $\mathbf{k}$  is the crystal momentum. The function  $u(x, t)$  has the lattice periodicity in  $x$ , and satisfies the transverse Schrödinger equation

$$i\hbar \frac{\partial u}{\partial t} = -\frac{\hbar^2}{2m\gamma} \frac{\partial^2 u}{\partial x^2} + V(x)u. \quad (2)$$

This can be derived starting from the Dirac equation; one then finds<sup>20</sup> that the transverse motion is nonrelativistic but that the electron has a relativistic mass  $m$ . The potential  $V(x)$  is that of a periodic set of continuous planes, and the potential of an individual plane can be taken<sup>17</sup> as the well-known atomic Doyle-Turner potential<sup>21</sup> averaged over a plane. Due to its lattice periodicity,  $V(x)$  may be expanded as

$$V(x) = \sum_m V_m e^{imgx} \quad (3)$$

where  $g$  is  $2\pi$  times the reciprocal lattice vector of the lattice of continuous planes (i.e.,  $g = \hat{x}/d$ , where  $d$  is the spacing of the planes). The wave function is expanded similarly,

$$u_n(x) = e^{ik_x x} \sum_m C_m^n e^{imgx}, \quad (4)$$

as first done by Bethe<sup>22</sup>; this later became known<sup>23</sup> as a "many-beam expansion." Equations (3) and (4) inserted into Eq (2) gives a set of linear equations

$$\sum_m A_{lm} C_m^n = E_{\perp}^n C_l^n, \quad (5a)$$

where

$$A_{lm} = \frac{\hbar^2}{2m\gamma} (k_x + lg)^2 d_{lm} + V_{l-m}. \quad (5b)$$

Truncation then transforms this into an eigenvalue problem for the transverse energy levels  $E_{\perp}^n$ , with  $C_l^n$  defining the eigenvectors.

As a generalization to three dimensions, we may note that Kurizki and McIver<sup>24,25</sup> chose to discard the spin effects of the electron which are known to be small, and thus to start from the Klein-Gordon equation instead of from the Dirac equation, i.e.,

$$\nabla^2 \psi + [(E - V)^2 - m^2] \psi = 0, \quad (6)$$

with  $c = 1$ . Retaining first-order terms in  $V/E$  only, and calling

$$U = 2EV = 2m\gamma V, \quad (7)$$

one has

$$\nabla^2 \psi + (E^2 - U - m^2) \psi = 0, \quad (8)$$

and, as before, one may expand (retaining this time the full three-dimensional geometry)

$$U = \sum_{\mathbf{g}} U_{\mathbf{g}} e^{i\mathbf{g} \cdot \mathbf{r}}, \quad (9)$$

$$\psi_{\mathbf{k}E}(\mathbf{r}) = \sum_{\mathbf{g}} c_{\mathbf{k}\mathbf{g}} e^{i(\mathbf{k} + \mathbf{g}) \cdot \mathbf{r}} \quad (10)$$

where

$$\mathbf{g} = 2\pi(n_1 \mathbf{b}_1 + n_2 \mathbf{b}_2 + n_3 \mathbf{b}_3), \quad (11)$$

$\mathbf{b}_i$  being the basic reciprocal lattice vectors and  $\mathbf{k}$  the crystal momentum. Inserting (9) and (10) into (8) leads to (calling  $E^2 - m^2 = k_0^2$ )

$$[k_0^2 - U_0 - (\mathbf{k} + \mathbf{g})^2] c_{\mathbf{k}\mathbf{g}} - \sum_{\mathbf{g}' \neq \mathbf{g}} U_{\mathbf{g}'} c_{\mathbf{k}, \mathbf{g} - \mathbf{g}'} = 0 \quad (12)$$

which is the three-dimensional analog of Eqs. (5) above and can be solved in a similar way, as an eigenvalue problem. Note that  $\mathbf{k}_0$  is the momentum vector of the electron outside of the crystal; the boundary conditions state that the components of  $\mathbf{k}_0$  tangential to the crystal surface are continuous, and agree with the tangential components of  $\mathbf{k}$ . Defining

$$D_{\mathbf{k}\mathbf{g}} = 2\mathbf{k} \cdot \mathbf{g} + \mathbf{g}^2 \quad (13a)$$

and

$$\varepsilon_{\mathbf{k}\perp} - k_{\perp}^2 = k_0^2 - U_0 - k^2 \quad (13b)$$

where  $\mathbf{k}$  is the transverse component of  $\mathbf{k}$  (i.e., normal to the channeling planes), it is found that  $\hbar^2 \varepsilon_{\mathbf{k}\perp} / 2m\gamma$  becomes the transverse energy eigenvalue  $E_{\perp}^n$  of (5a) if the

continuum approximation for the channeling planes is made.<sup>25</sup> Equations (13) transform (12) into

$$(\varepsilon_{k_{\perp}} - k_{\perp}^2 - D_{k_{\perp}})c_{k_{\perp}} - \sum_{g' \neq g} U_{g'} c_{k_{\perp} - g'} = 0. \quad (14)$$

This is an eigenvalue problem for  $\varepsilon_{k_{\perp}}$  (but note that for the three-dimensional, i.e., noncontinuum case,  $D_{k_{\perp}}$  also contains this eigenvalue!) and for the eigenvectors  $c_{k_{\perp}}$ .

The solutions for the one-dimensional case, Eqs. (5), have been obtained in Ref. 26, the corresponding transverse energy eigenvalues  $E_{\perp}^n$  for 4-MeV electrons channeled along the (110) plane of Si are shown in Fig. 10 in a reduced Brillouin-zone scheme, plotted versus the angle  $\theta$  of the incident electron with the channeling plane; the units are in eV for the transverse energy eigenvalue in the electron rest system. The atomic Doyle-Turner potential<sup>21</sup> was averaged over the continuous (110) plane, as in Ref. 19, with which the results of Ref. 26 agree very well. In addition the eigenvectors  $C_1^n$  were obtained, which need to be known for calculation of the populations of the excited states and of the radiation intensities. The quantities  $E_{\perp}^n$  and  $C_1^n$  also were obtained in Ref. 26 for 56-MeV electrons along the (110) direction of Si, using an appropriately averaged Doyle-Turner potential. The bound-state energy levels agree very closely with the results of the tight-binding approximation as used in Ref. 20. It should be noted that the periodic crystal potential,  $V(x)$  of Eq (3), i.e., that of a periodic set of continuous planes, has a DC component which was chosen in Ref. 26 as the reference value for the energy scale. In other words, an appropriate offset was subtracted from the transverse energy eigenvalues  $E_{\perp}^n$ , which, for 4-MeV electrons in Si, amounts to 63.55 eV, in order to arrive at the level diagram of Fig. 10.

One also can calculate the populations of the  $n$ th channeling state  $\psi_{kn}$  as they are initially established by a plane wave  $\psi_{pw}$  incident upon the crystal. This plane wave can be expanded in terms of the set  $\psi_{kn}$ ,

$$\psi_{pw} = \sum_m A_m \psi_{km}, \quad (15)$$

the populations then being

$$\pi_n = |A_n|^2. \quad (16)$$

For the one-dimensional Bloch-function case, this simply becomes (in the first Brillouin zone)

$$\pi_n = |C_0^n|^2. \quad (17)$$

For the case of the tight-binding approximation, the appropriate formulas for  $\pi_n$  are given in Ref. 20. The populations of the bound levels  $n = 0$  to 5 for that case are shown in Fig.

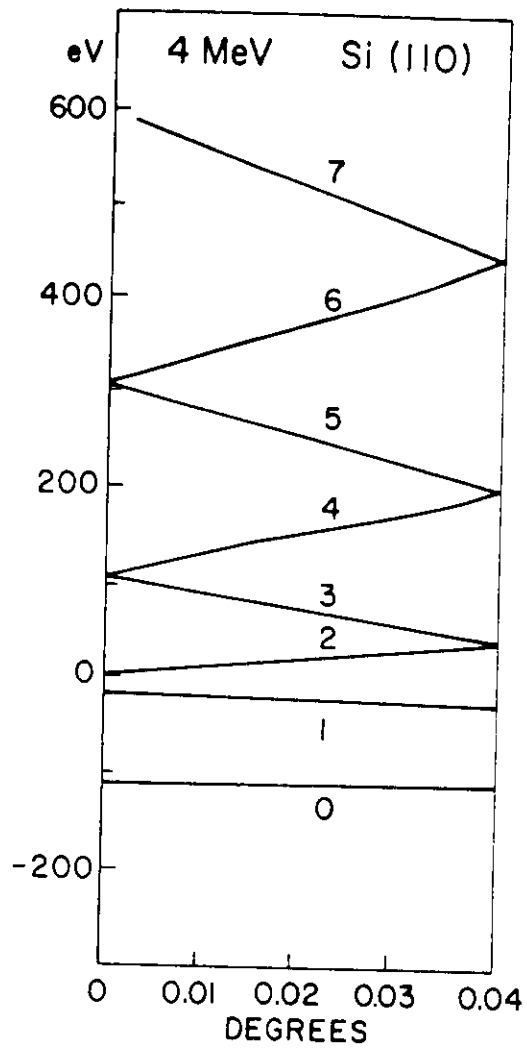


Figure 10:

Energy bands for 4-MeV electrons channeled along the (110) plane of Si. The energy in the rest system of the electrons (units eV) is plotted versus  $k_x$ , as given in terms of the angle of the incident electron with the channeling plane (in degrees).

11 (solid lines), referring to 56-MeV electrons in the (110) channel of Si. The scales of these figures are arbitrary; their normalization is given in Fig. 4 of Ref. 20.

Having these tight-binding results for the channeling-state populations, one may now compare with them the results of the one-dimensional Bloch-function calculation based on Eq (17). For the 56-MeV electrons along the (110) planes of Si, these are shown as dashed curves in Fig. 11 for  $n = 0$  to 5. The dashed curves are normalized to the scale shown. Comparing the solid and the dashed curves, we see that the results are qualitatively similar. If one now considers 4-MeV electrons in the (110) channel of Si, one obtains Fig. 12, which can be compared with Andersen's<sup>19</sup> populations based on Bloch functions, and is seen to be very similar as well.

Reference 20 presents the formula for the channeling radiation intensity,  $dI = qd\sigma$ , which for forward emission is

$$\frac{m^2}{L} \frac{dI}{d\Omega_{\mathbf{k}|_{nn'}}} \Big|_{\text{forw}} = \frac{e^2}{2\pi} \frac{q^2 |p_{nn'}|^2 \pi_n(\theta)}{E^2 (1 - \beta_{\parallel} \cos \theta)} \left( \cos \theta - \beta_{\parallel} \frac{q_{nn'}}{\omega_{nn'}} \sin^2 \theta \right)^2, \quad (18)$$

where  $L$  is the crystal thickness,  $q$  is the photon momentum,  $E$  is the total energy of the incident electron and  $\omega_{nn'}$  is the transition energy between transversely bound states. Furthermore,  $\beta = k/E$  where  $k = k_0 \cos \theta$ ,  $E = (k^2 + m^2)^{1/2}$ , where  $k_0$  is the incident electron momentum, and  $p_{nn'}$  is the dipole transition matrix element. The intensity is concentrated in lines located at

$$q_{nn'} = \frac{\omega_{nn'}}{1 - \beta_{\parallel} \cos \theta}. \quad (19)$$

The line intensities are best described by a line strength factor

$$f_{nn'} = D_n |p_{nn'}|^2 \pi_n \quad (20)$$

where  $D_n$ , the "depletion factor" is a measure of the depopulation of the channeling states by dechanneling; it has been obtained empirically and is quoted in Ref. 20.

The dipole matrix elements  $p_{nn'}$  were calculated in Ref. 20 for the tight-binding-approximation case. A calculation of the radiation matrix element based on Bloch functions is given by Kurizki and McIver<sup>24,25</sup> with these results: if the radiation matrix element is designated by<sup>27</sup>

$$J_{\lambda}(\mathbf{q}) = \mathbf{j}(\mathbf{q}) \cdot \boldsymbol{\varepsilon}_{\lambda}^*, \quad (21)$$

where

$$\mathbf{j}(\mathbf{q}) = \int \psi_n^*(\mathbf{r}) \boldsymbol{\alpha} \psi_n(\mathbf{r}) e^{-i\mathbf{q} \cdot \mathbf{r}} d^3r, \quad (22)$$

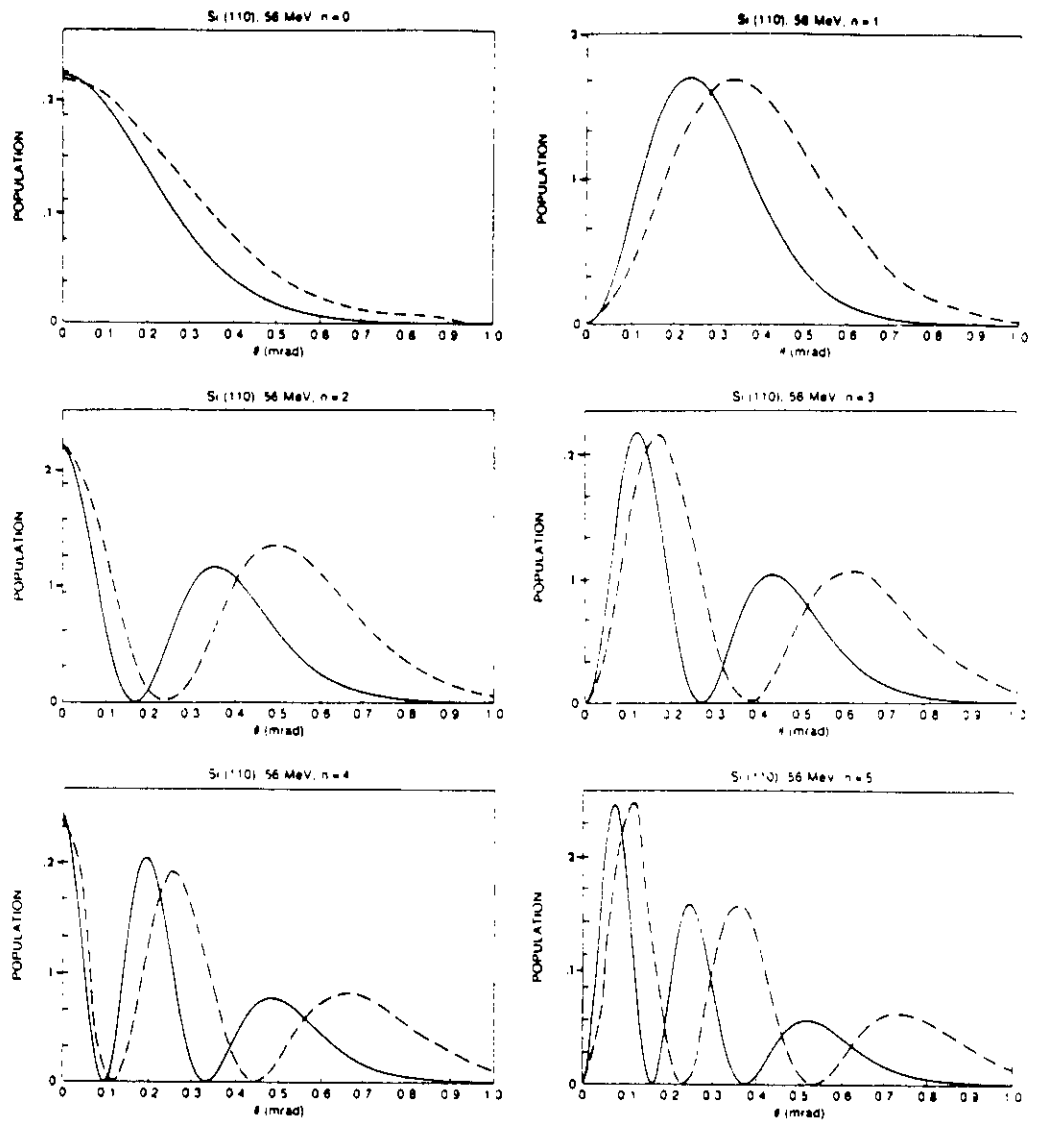


Figure 11:

Populations of electron channeling states  $n$  along the (110) plane of silicon, generated by 56- MeV incident electrons ( $n = 0$  to 5, read left to right and downward), calculated in the tight-binding approximation (solid curves) and using one-dimensional Bloch functions (dashed curves).

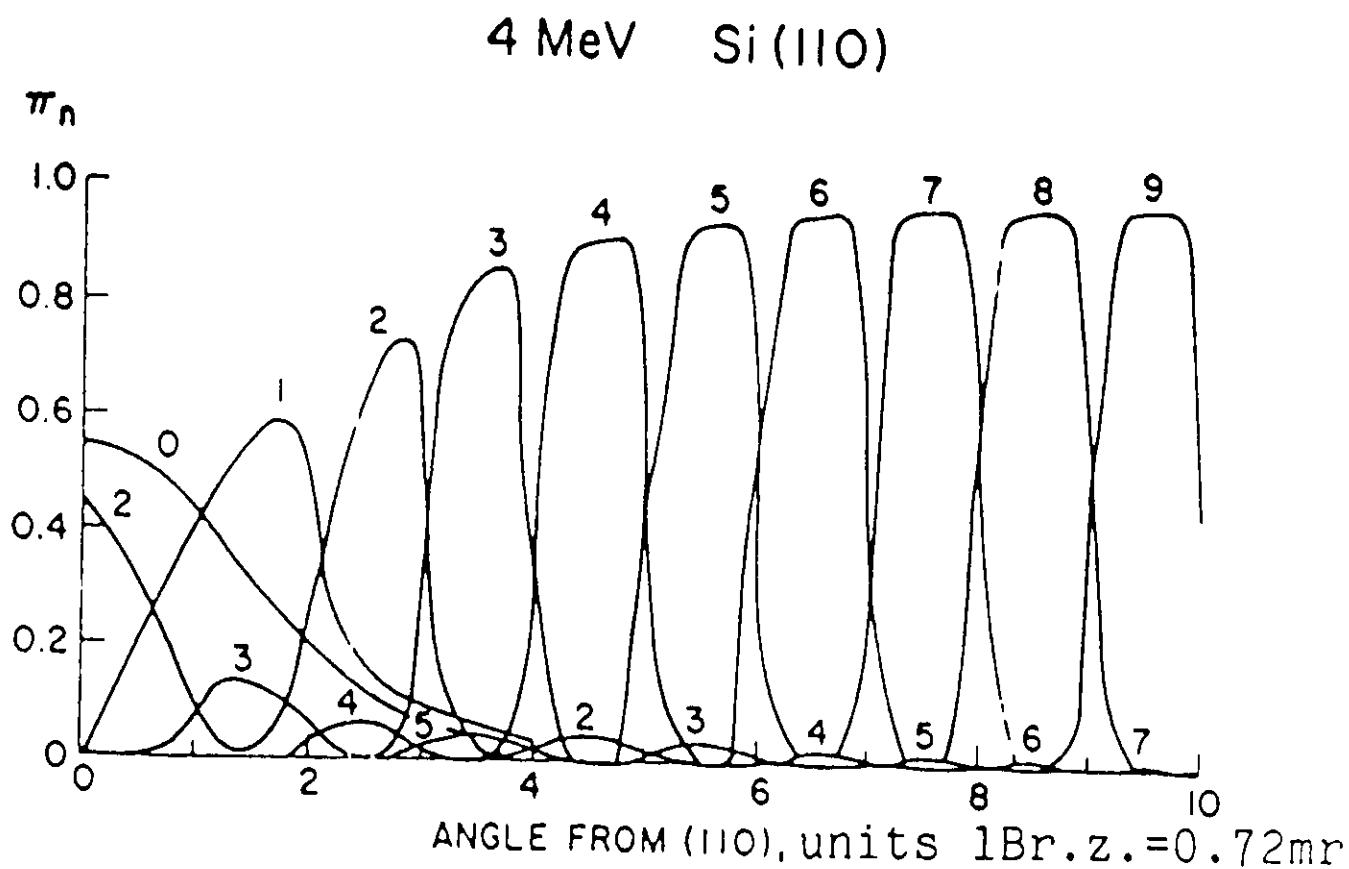


Figure 12:

As in Fig. 11 (dashed curves), for 4- MeV electrons.

then the use of Bloch-Dirac functions of Eq (10), dropping the magnetic terms, gives

$$\mathbf{j}(\mathbf{q}) = \frac{\hbar}{\gamma mc} \sum_{\mathbf{g}} (\mathbf{k}_0 + \mathbf{q}) c_{\mathbf{g}}^{(n)} c_{\mathbf{g}+\mathbf{K}}^{(n)*} \delta(\mathbf{k}_0 - \mathbf{k}_f - \mathbf{q} - \mathbf{K}) \quad (23)$$

where  $\mathbf{k}_f$  is the final electron momentum and  $\mathbf{K}$  the momentum transfer to the lattice.

Equation (23) can be specialized in a straightforward manner to the one-dimensional case. The strength factor  $f_{nn'}$  can be calculated from this and compared with the results for  $f_{nn'}$  based on the tight-binding approximation for a Si lattice. The comparison is given in Fig. 13, where the tight-binding approximation results are shown as the bars on the right and the one-dimensional Bloch-function results as the bars on the left. (These latter data are not absolute, but are normalized to  $\theta = 0.2$  mrad for the  $1 \rightarrow 0$  transition in Si.) The energy differences for the two calculations are too small to be apparent in the figure. It is seen that there is good overall agreement between the results of the two calculations, but that some differences do appear between the tight-binding results and the presumably more accurate results of the Bloch function calculation. While the matrix elements are found not to deviate in any essential way, the bulk of the differences can be traced to differences in the populations. This is evident from Fig. 11, and is caused by the great sensitivity of  $\pi_n(\theta)$  to variations in  $\theta$ . This renders channeling radiation a sensitive measure for the populations in channeling states. The excellent emittance of modern electron accelerators makes it possible to take advantage of the oscillations of population shown in Figs. 11 and 12: In fact, the population inversions apparent in the figures open the possibility of producing a CR x-ray laser.

Various processes affect the intrinsic features of the CR lines as they appear in Fig. 13. In this figure, forward emission only is shown, using a detector of very small opening angle ( $< 0.1$  mrad). If the full radiation cone (opening angle  $\sim 1/\gamma$ ) is observed, the CR peaks are spread out as in Fig. 9(c). However, even for forward emission and detection, CR peaks show a certain width which is evident in all experimental spectra. Decreases in intensity and even level shifts are sometimes observed as well.

A detailed discussion of the relevant effects is given in Refs. 17, 28, and 29. Electrons are channeled over a finite distance only, called the channeling length or coherence length  $\Lambda$  (coherence length because over this distance the emitted CR is coherent), which may or may not be smaller than the crystal thickness.

The main cause of dechanneling is collisions with atomic nuclei (especially due to the thermal vibrations of the latter), but also results from scattering by electrons and (less importantly) by defects. The corresponding coherence lengths are  $L_n$ ,  $L_e$ , and  $L_d$ , respectively. The total mean free path  $\Lambda$  is then given by

$$\Lambda^{-1} = L_n^{-1} + L_e^{-1} + L_d^{-1}. \quad (24)$$

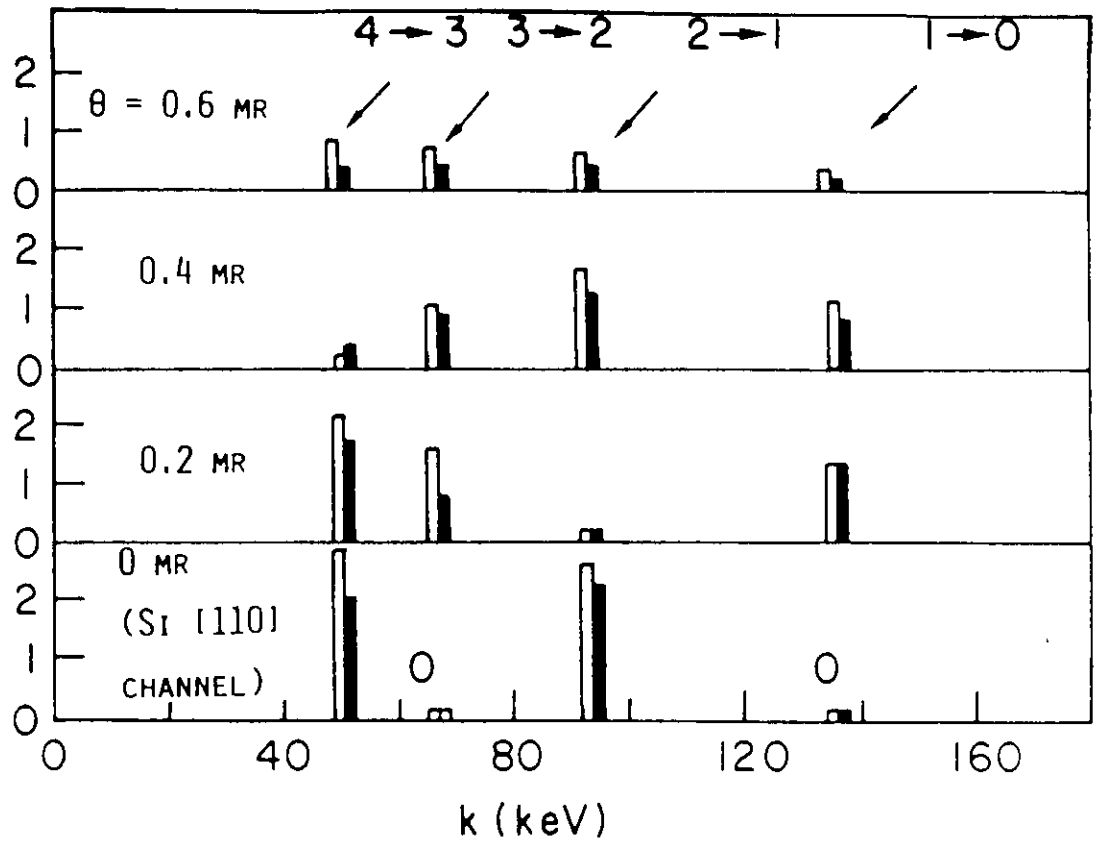


Figure 13:

Change in intensity of most prominent CR spectral intensity peaks, as a 56-MeV incident electron beam rotates in the (001) plane away from the [110] channel direction of Si ( $\theta = 0.6$  mr), 0 being measured from the [110] direction in the (001) plane, with results of one-dimensional Bloch function calculation added as the left-hand bars.

Dechanneling causes the initially established populations of the different channeling states to vary as the electrons propagate through the crystal, as can be seen in Fig. 14. The radiation matrix element decays with depth  $z$  as  $\exp(-z/2\Lambda)$ , and for forward emission, the photon yield has the form

$$I(\omega) \propto (\sin x/x)^2, \quad (25)$$

where  $x$  is proportional to  $\Delta\omega$  (the photon energy measured from the line center) and to the mean free path. The resulting line is a Lorentzian with width<sup>17</sup> (for  $\gamma \gg 1$ ):

$$\text{FWHM} \cong 2\gamma^2/\Lambda, \quad (26a)$$

except for the case when the crystal thickness is less than  $\Lambda$ , when

$$\text{FWHM} \cong 3.5\pi\gamma^2/L. \quad (26b)$$

In addition to this intrinsic line width, a Gaussian detector response contributes and has to be folded in<sup>28</sup> to obtain the effective line shape.

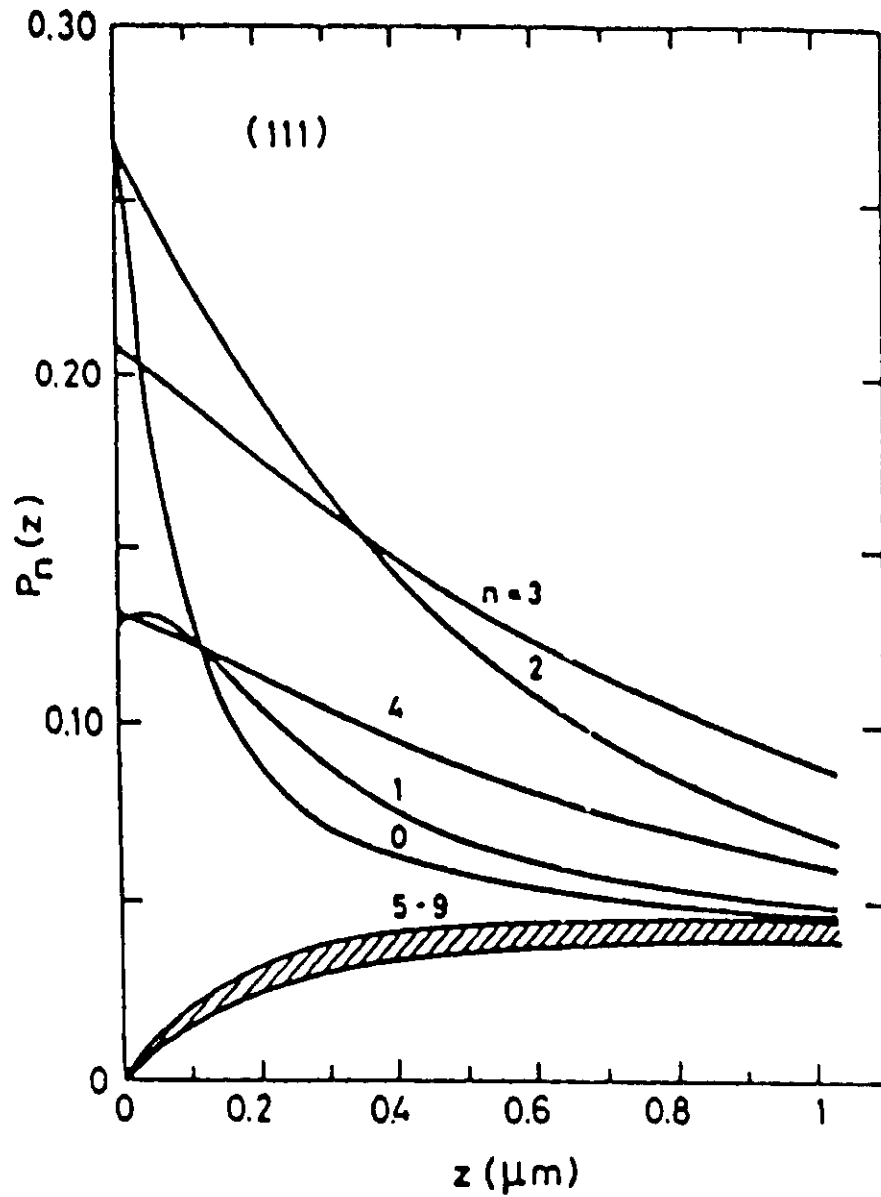


Figure 14:

Depth dependence of the population of different bands  $n$  for 4- MeV electrons incident at an angle of half the Bragg angle,  $\psi_B/2$ , with a (111) plane in Ni at room temperature.

## 5. USE OF CHANNELING RADIATION FOR X-RAY LITHOGRAPHY

Lithography is the technology of producing, or mass-producing, microcircuits (chips) by optical exposure of a light-sensitive material called a resist, through a mask that contains the microcircuit pattern.

After exposure, the exposed portions (or alternatively, the non-exposed portions) of the resist are chemically dissolved and removed from its backing, which generally consists of a thin silicon wafer. This technique has so far been carried out with intense optical or ultraviolet light; but with the present demand for high-density chips with a submicron pattern, optical lithography has reached its limits due to diffraction, and the use of x rays has been called upon. For such a purpose, synchrotron-generated x rays have been considered,<sup>30,31</sup> with typical energies of 0.5-3 keV (a strict monochromaticity of the x rays is not required), and IBM has set up an experimental station based on a \$25M synchrotron with ten beam ports; all the activities there during the last ten years, including mask technology, have so far led to expenditures of \$500M.<sup>32</sup> Alternate high-intensity x-ray sources that are not based on expensive synchrotrons are clearly desirable, and one source, transition radiation (TR), produced by an electron beam incident on a stack of thin foils, has been tested at Livermore for application to lithography.<sup>33</sup>

Figure 15 shows a series of plasma or electron-beam based processes (and their required energies) that are capable of producing x rays in the keV region, as discussed by Hollman.<sup>34</sup> Wedell<sup>35</sup> suggested the use of CR for lithography in 1980, and estimated that with a 1-2 MeV linac of several kW power, 0.1 photon would be emitted per electron, leading to exposure times of wafers of as little as a few minutes.

For x-ray lithography, a typical setup, used in the Livermore TR experiment,<sup>33</sup> is shown in Fig. 16. The important quantity is the exposure time. Hollman<sup>34</sup> has given some estimates of these times. Under his assumed conditions, synchrotron radiation looks favorable. However, his assumed conditions cast doubt on these single-parameter comparisons. Hollman considered synchrotron, laser plasma, pinch plasma, transition radiation, and conventional (incoherent) bremsstrahlung (IB). His results are shown in Table I. He assumed a PMMA resist of sensitivity 1 J/cm<sup>2</sup>, a 2- $\mu$ m silicon mask, and a 25- $\mu$ m beryllium window.

Sprangle *et al.*<sup>36</sup> proposed a scheme of using electromagnetic waves as an undulator in an electron storage ring. Wedell<sup>35</sup> considered channeling radiation, and his conclusion was that channeling radiation could be competitive with synchrotron radiation. Their results are shown in Table II.

In these comparisons, one needs to look at how these parameters were obtained. The exposure time,  $T_E$ , is the resist sensitivity (in J/cm<sup>2</sup>) divided by the absorbed areal power density (in W/cm<sup>2</sup>). The resist sensitivities have been given for PMMA in Refs. 34 and 36 as approximately 1 J/cm<sup>2</sup> and for PGMA in Ref. 33 as 0.06 J/cm<sup>2</sup>. Several of these estimates used PMMA, which is relatively insensitive. Newer resist materials, such

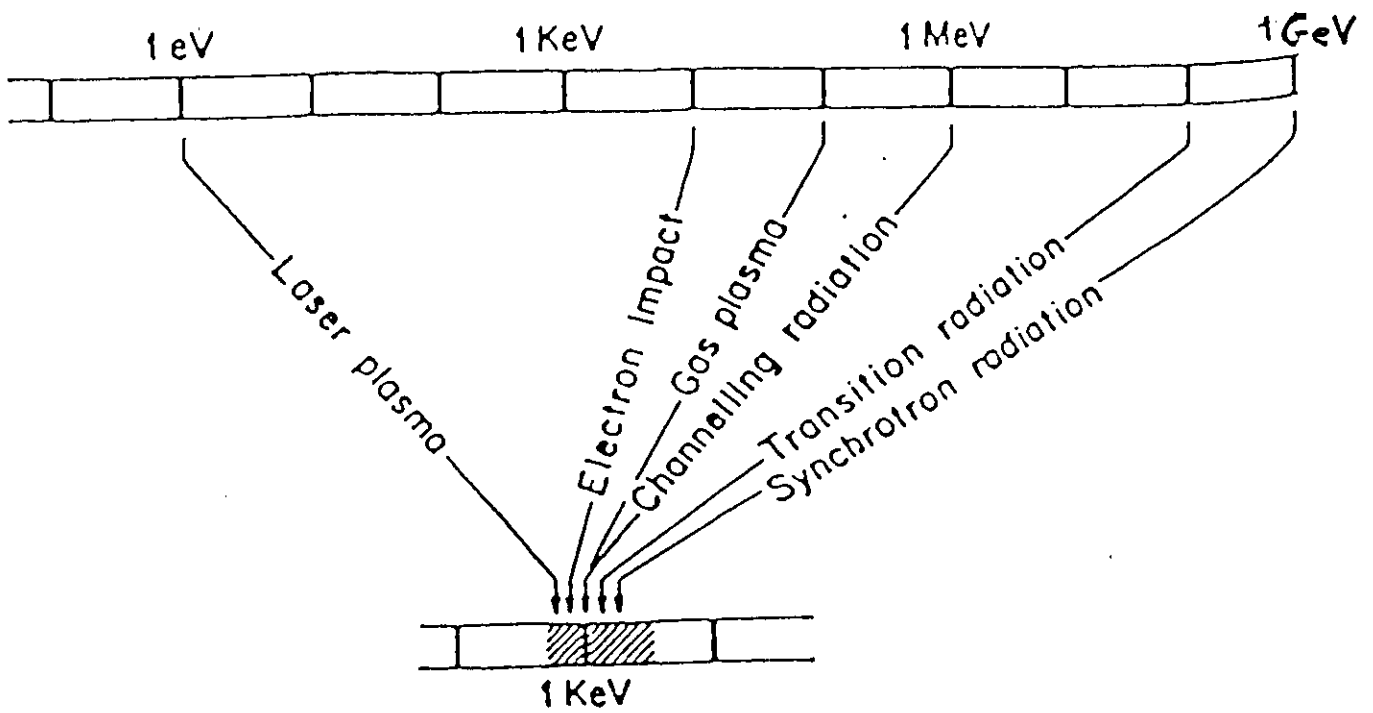


Figure 15:

Energy conversion processes producing soft X rays.

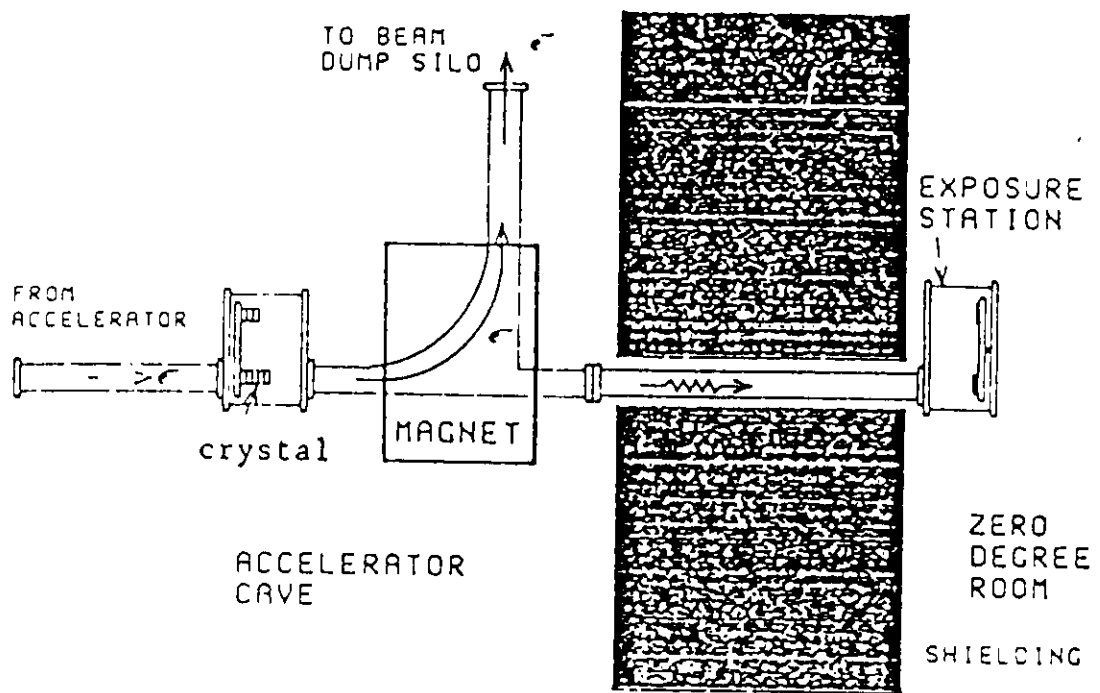


Figure 16:

X-ray lithography setup.

**Table I. Previous Comparisons <sup>34</sup> of Wafer Exposure Times in X-ray Lithography for Various X-ray Sources (d = source - wafer distance).**

<u>Source</u>	<u>Parameters</u>	<u>Exposure Times (s)</u>
Synchrotron	E = 1 GeV B = 23 kG i = 300 mA d = 5 m	8.1
Laser Plasma	10 J/pulse @ 10 Hz d = 20 cm	266
Pinch Plasma	Gas: Kr 10 W av. power d = 20 cm	175
Transition Radiation	E = 100 MeV i = 1 mA 25 foils, 0.5 $\mu$ m Be d = 5 m	1497
Conventional IB	Anode: W V = 10 kV i = 1 A d = 20 cm	12120

**Table II. Additional Comparisons.**

<u>Source</u>	<u>Parameters</u>	<u>Exposure Times (s)</u>
EM wave Undulator <sup>36</sup>	E = 250 MeV i = 500 mA d = 8.5 m	12.3
Channeling Radiation <sup>35</sup>	E = 1-2 MeV W crystal P = 1 kW	100-300

as PGMA, have much higher sensitivity. With technological advances in resist sensitivity, comparisons done with today's practice may not be relevant.

The ultimate figure of merit<sup>37</sup> is the throughput,  $T$ , which is the number of wafers that can be processed per hour:

$$T = 3600/[T_{LU} + T_G + (A_W/A_C)(T_S + T_A + A_C^{1/2}/V + T_E)].$$

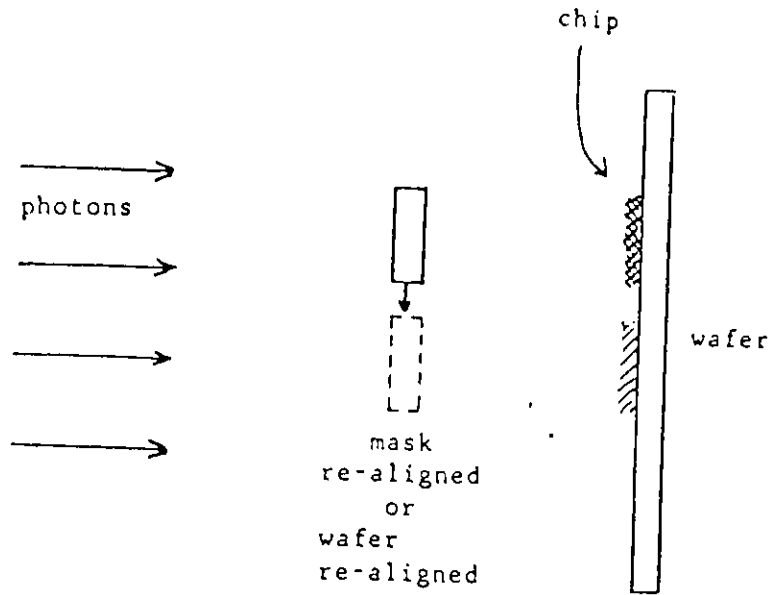
The exposure time enters through the last term in the denominator. The other parameters in this equation are  $T_{LU}$ , the wafer load/unload time (20 s);  $T_G$ , the global alignment time (6 s);  $T_S$ , the stage acceleration and settle time ( $1/4$  s);  $T_A$ , the chip alignment time ( $1/2$  s);  $V$ , the stage velocity ( $1/2$  cm/s);  $A_W$ , the wafer area (5-inch diameter); and  $A_C$ , the chip area ( $3 \times 3$  cm<sup>2</sup>).

Let us look at what is meant by the throughput formula. First the wafer has to be put into the photon beam (see Fig. 17). Then the wafer is realigned for each chip. Effectively, the mask is moved about to write many chips on the wafer. If the photon beam is wide enough, and if masks could be made complex enough to write multiple chips, then there is a different dependence on the exposure time. The elimination of the aligners/steppers, which cost in excess of \$1 million each, could produce large savings; further, no time need be wasted in positioning the wafers.

In Fig. 18, we present plots of throughput versus exposure time. In Fig. 18a, the lowest curve was obtained with the above formula. However, if we eliminate the need to realign the wafer to write each chip in turn, we see a dramatic increase in throughput. Figure 18b shows the same calculation, but presented differently. Eventually, the exposure time becomes the dominant time dependence, but the biggest improvement can be made if the whole wafer could be written at one and the same time. This would be the case with channeling radiation.

From the existing data, we make some estimates of the exposure time and throughput for the channeling radiation from several low-energy accelerators, namely the Darmstadt linac,<sup>9</sup> the commercially available Varian Linatron, and the CEBAF injector, in Table III. We assume that a tungsten crystal target is used with all of these linacs, because the channeling-radiation intensity from tungsten surpasses that from silicon or diamond<sup>10</sup>; tungsten can be used here since the lack of monochromaticity is of no adverse consequence for x-ray lithography. With the CEBAF injector linac, exposure times for CR are less than the synchrotron values, even for conventional chip realignment.

The Varian accelerator is commercially available, but its beam divergence  $\Delta\theta_e$  is greater than the Lindhard angle (the limiting angle, within which electrons are trapped into channeling orbits). For the Darmstadt and CEBAF accelerators, the entire beam would be channeled.

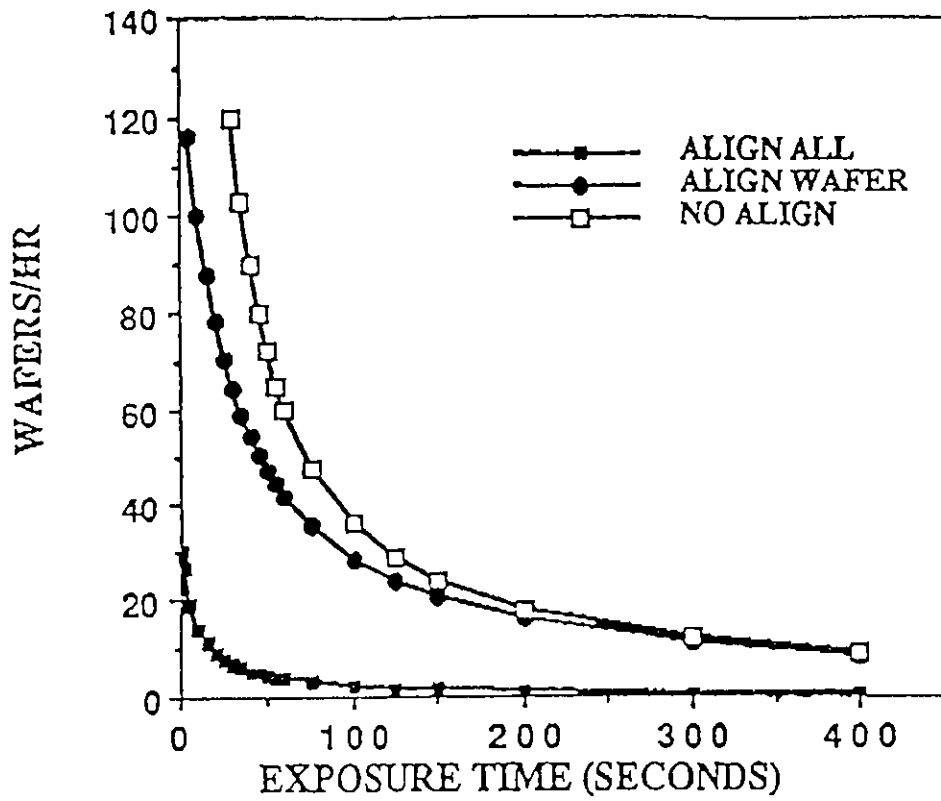


$$\left. \begin{aligned} \frac{A_w}{A_c} &= 1 \\ T_s + T_A + \frac{\sqrt{A_c}}{V} &= 0 \end{aligned} \right\} \begin{array}{l} \text{if large enough} \\ \text{mask can be made} \\ \text{to write multiple} \\ \text{chips} \end{array}$$

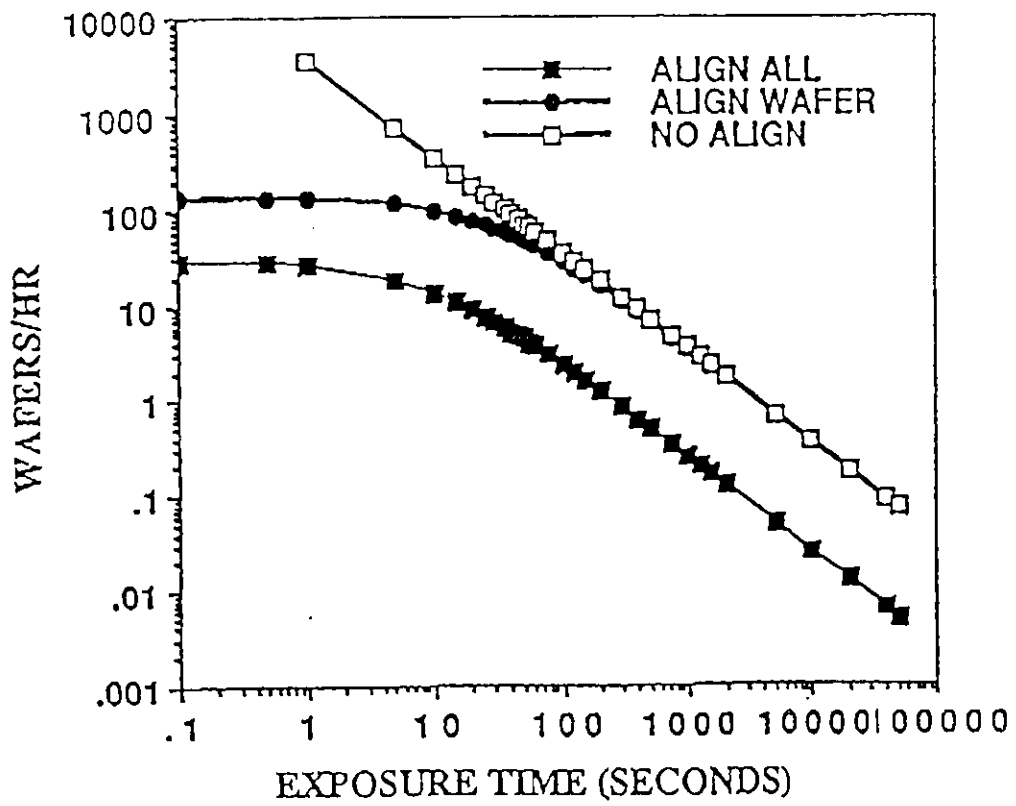
$$T_{L/U} + T_G \rightarrow 0 \quad (\text{or very small}) \text{ if mechanics improved.}$$

Figure 17:

X-ray lithography with wafer realignment.



a



b

Figure 18:

Wafer throughput.

Table III. Channeling Radiation Estimates  
 $T_E$  (seconds); T (wafers/hr.)

Parameters (d = 1.5 m)	With Chip Realignment		Without Chip Realignment	
	PMMA	PGMA	PMMA	PGMA
<u>Darmstadt Linac</u>				
E = 5 MeV	500 s	30 s	500 s	30 s
i = 30 $\mu$ A	0.5/hr	8/hr	7/hr	107/hr
$\Delta\theta_e = 0.05$ mrad				
<u>Varian Linatron</u>				
E = 6 MeV	150 s	9 s	150 s	9 s
i = 100 $\mu$ A	2/hr	15/hr	24/hr	500/hr
$\Delta\theta_e = 1$ mrad				
<u>CEBAF Injector Linac</u>				
E = 5 MeV	93 s	5.5 s	93 s	5.5 s
i = 200 $\mu$ A	3.5/hr	20/hr	40/hr	650/hr
$\Delta\theta_e < 0.1$ mrad				

Note that the throughput of the undulator source (Table II) is 12 wafers/hour. This is less than our CR estimate for the CEBAF injector linac. Similarly, our channeling-radiation throughput estimates compare favorably with those of the other sources, listed in Table I.

Even more important, the use of the wider channeling-radiation beam eliminates the need for steppers and alignment, and the entire wafer can be exposed at once. Therefore, the last column of Table III applies, and the results show a dramatic improvement in favor of channeling radiation; with the CEBAF linac, one can obtain a throughput as high as 650 wafers/hour. Moreover, in this case, one could easily afford to use a PMMA resist, which has better resolution than PGMA.

One point to be mentioned is that the wider divergence ( $\Delta\theta \sim 1/\gamma$ ) of the CR beam, although eliminating the need for steppers, might cause a lack of definition in the peripheral areas of the wafer. This could cause a problem with the etching of deep channels, but even this deficiency might be alleviated by employing Kumakhov's x-ray focusing device,<sup>38</sup> which can parallelize a divergent beam, albeit with significant loss of intensity. Another point is that the  $\theta \sim 1/\gamma$  opening half-angle of CR permits the exposure as a whole of a 12-inch wafer at a distance of only 1.5 m from the source. Wafers of this size are likely to become the industry standard within the next decade.

Finally, compared to synchrotron radiation, CR appears to be much more advantageous not only due to its higher throughput (Table III), but also because of the lower cost of the facility: a suitable electron linac would cost far less than the \$25-50M for a few-GeV synchrotron.

## 6. EXPERIMENT

We propose to set up a beam line at the output of the 5-MeV stage of the injector. The beam line that we have designed is shown in Fig. 19. It is designed with several purposes and constraints in mind:

1) It can be used with both low- and high-intensity electron beams, the former (in the nanoamp range) to enable us to do counting experiments without excessive pileup (the cross sections involved are megabarns!), and the latter (in the 100-microamp range) to enable us to perform exposures of objects for which a large integrated radiation dose (of the order of hundreds of millijoules), such as a silicon wafer to be etched, is necessary. The great advantage of a high-duty-factor beam is that one does not need to use picoamp beams to avoid pileup, as was necessary at Livermore and elsewhere, and the resulting gain in counting rate enables high-statistics spectra to be acquired in a matter of minutes, even with small solid angles and low-efficiency detectors.

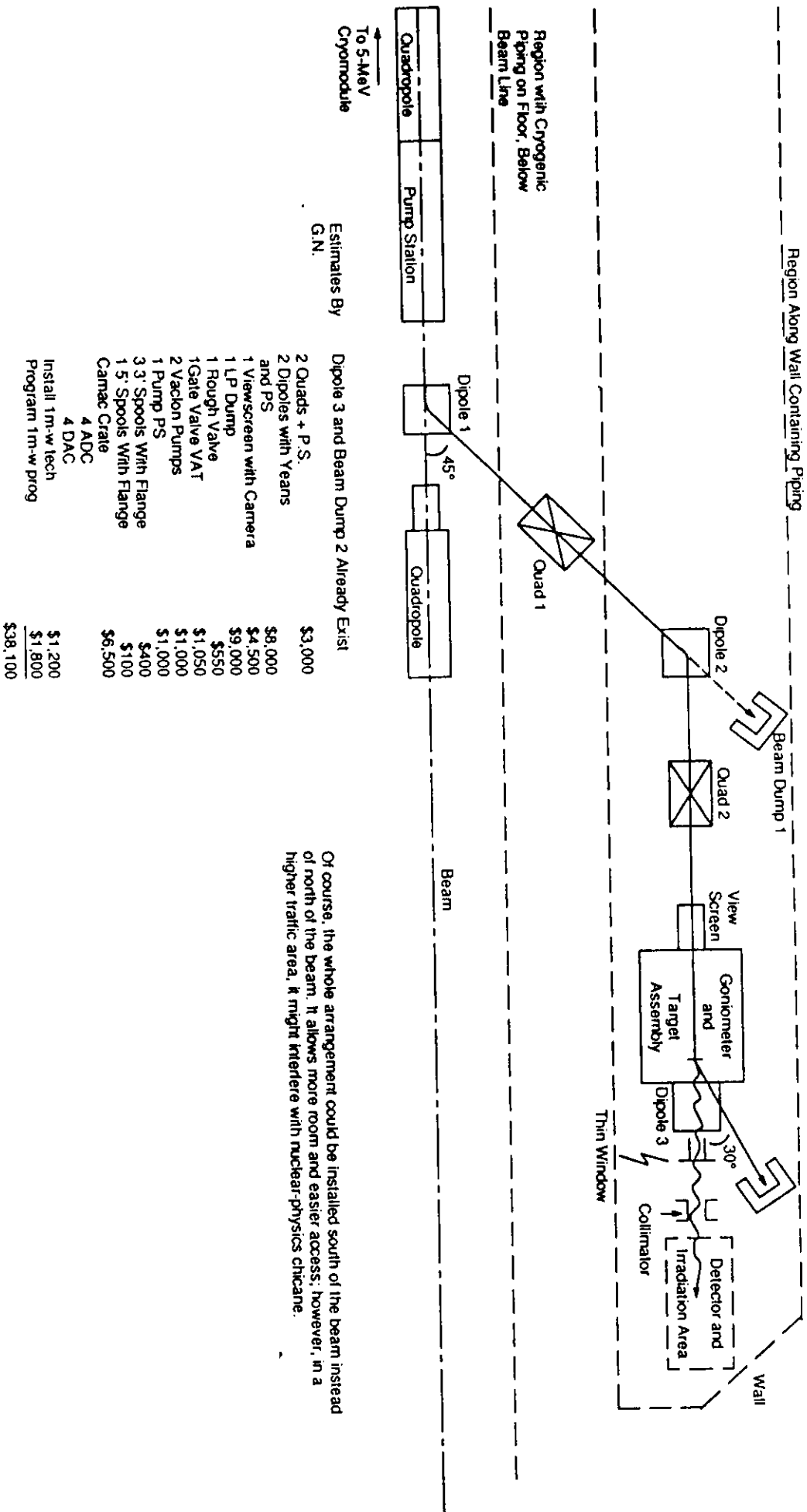
2) It can be accommodated in the limited space available between the 5-MeV section and the shielding wall upstream of the 40-MeV section and between the main accelerator beam line and the wall. This latter constraint is particularly important in view of the high density of equipment planned for use in this area.

The proposed beam line (see Fig. 19, which also gives a cost analysis) consists of two dipoles for a parallel translation of the beam and a number of quadrupoles for focusing. A sweeping magnet directs the electron beam, after it passes through the crystal target, into a Faraday cup, feeding a charge integrator, to monitor the electron beam intensity. Steering coils will be added as necessary. Some of these elements already exist at CEBAF, and the rest will be purchased by SFA immediately upon approval of this proposal. A goniometer holds the single-crystal targets; one possible instrument is the one used at Livermore--a three-axis goniometer capable of 0.02-mrad steps, remotely controlled. Photon spectra will be acquired with a high-resolution solid-state spectrometer, probably a Si(Li), but possibly a Ge(Li) or intrinsic HPGe detector. Both of these elements will be provided by SFA as well. Electronics and computer interfacing will be conventional, and will be provided by GWU. Cabling to the data-collection station, and the station itself, will be provided by CEBAF. Analysis of the data will be carried out at GWU and/or CUA.

We envision using single-crystal targets of silicon, diamond, and tungsten, to be provided by SFA and/or Sandia. Silicon crystals are inexpensive, easily obtained, and well studied, so that they will be used for setup and calibration runs. Diamond has the highest Debye temperature; hence the spectral lines are sharpest, and will be used for resolution studies and for those runs which require a monochromatic beam. Tungsten, having the highest atomic number, should produce radiation spectra of the highest intensity, and hence should be most useful for high-intensity applications runs.

We propose essentially two kinds of experimental runs--low-intensity and high-intensity. The low-intensity runs will be for setup, calibration, alignment and resolution,

Figure 19: Low-Energy Channeling-Radiation Beam Line



Of course, the whole arrangement could be installed south of the beam instead of north of the beam. It allows more room and easier access, however, in a higher traffic area, it might interfere with nuclear-physics chicane.

will be for applications. The primary applications runs will test the feasibility of using channeling radiation as an x-ray source for submicron lithography. For these runs we plan to expose both small- and large-area silicon wafers; the wafers, masks, and resists will be provided by SFA. We hope also to be able to perform an exploratory run for the application of channeling radiation to problems in medical diagnostics, notably angiography. The phantom(s) and film needed for such a run also will be provided by SFA.

In the interest of retaining a capability for future experiments at CEBAF (see Sec. 8 below) after the conclusion of the measurements proposed here, SFA agrees to donate the experimental it will have provided to CEBAF.

## 7. BEAM REQUIREMENTS

The electron-beam requirements for these measurements are:

- (1) Energy variable from 2.5 to 5.5 MeV;
- (2) Intensity variable from 1 to 10 nA for low-intensity runs, from 0.05 to 0.2 mA for high-intensity runs;
- (3) Duty factor as high as possible, but at least 20%, for low-intensity runs; no requirement for high-intensity runs;
- (4) Emittance as low as possible for all runs; maximum emittance is a function of crystal species and orientation--the most stringent requirement is for axial channeling of 5.5-MeV electrons in diamond, for which the maximum allowable emittance is 2 mm-mrad.

It is now clear why the CEBAF 5-MeV injector is the world's best facility for channeling-radiation experiments--the combination of high current, high duty factor, and low emittance available at CEBAF is unparalleled.

In assessing the counting rates for these kinds of measurements, some of the usual criteria are not applicable. For obtaining radiation spectra, for example, one is not count-rate limited, as with essentially all types of nuclear-physics experiments--a data run takes only a few minutes. Rather, the critical factors governing the amount of beam time needed depend on how long it takes to align the equipment, reduce backgrounds, and get control over systematic uncertainties. These factors are hard to assess in advance of the implementation of a new facility; but our experience at several other facilities dictates that we plan on at least 10 shifts (80 hours), split into a number of short running periods over a time interval of perhaps a few weeks, to make the facility operational (after the beam-line elements have been installed and surveyed into position). Low-intensity runs then are expected to occupy an additional 5 shifts, preferably during a single week. Setting up for the high-intensity runs, where we shall be concerned with questions of extrapolation from low to high intensities, of reproducibility, and of monitoring and safety issues (here it should be noted that the beam energies we plan to use lie below the photoneutron thresholds in nearly all materials), can be expected to require about 3 shifts. Finally, data acquisition at high intensities, where counting rates are measured in terms of currents rather than individual events, will require no less than 6 shifts, divided into no more than 2 periods (of 24 hours each). Setting aside a shift for some unforeseen contingency (other than any accelerator malfunction), we reach a total of 25 shifts (200 hours).

## 8. FUTURE PROSPECTS

Although the following prospective measurements are not part of the present proposal, the existence of a functional low-energy electron-beam facility suitable for the study of coherent radiation sources opens up the possibility of a wide variety of future experiments. In particular, fundamental physics studies, which are not emphasized in the present proposal, play a prominent role. These basic studies can take three forms:

(1) Continued and extended studies of channeling radiation. The beam line proposed here will be a qualitatively better facility for channeling-radiation studies than any previous one. One therefore can look forward to producing qualitatively better and more extensive data, with consequent unforeseen advances in the field, akin to the qualitative advances in nuclear spectroscopy made possible by the development of solid-state gamma-ray detectors which were capable of much higher resolution than the previously existing inorganic scintillators.

(2) More detailed studies of types of coherent radiation that are already well known. Among these are coherent bremsstrahlung and transition radiation, and the interferences among these and channeling radiation. The beam line proposed here will give us a more accurate tool to observe predicted but heretofore unseen phenomena.

(3) Studies of new kinds of coherent radiation. These include Smith-Purcell radiation, parametric x-ray production, coherent Cerenkov radiation, and several others.<sup>39</sup> Since very little is known about these types of coherent-radiation sources, much can be learned with a state-of-the-art ultralow-emittance electron-beam facility.

It is important to note that for all of the above, the study of polarization phenomena has been just at or more often just beyond the state of the art. There is no doubt that a wide variety of polarization measurements will have an important impact on our insights into and understanding of coherent-radiation phenomena, again very likely with currently unforeseen results.

Yet another frontier lies in the study of coherent-radiation phenomena on synthetic crystals, tailor-made to enhance the production or tuning of channeling or some other kind of coherent radiation. Promising examples are superlattices, either of the strained-layer variety using elements of the same valence structure, such as silicon and germanium, or those of mixed atomic species, such as the III-V compounds, including GaAs, InP, and others. Such crystals now can be grown epitaxially, one atomic layer at a time, thus enabling one to prescribe a crystal species with a desired characteristic. Coherent effects involving the long-range periodicity of such crystals along the electron-beam direction, such as longitudinal channeling radiation, which is predicted to be an order of magnitude more intense than ordinary channeling radiation,<sup>40</sup> can be produced.

Applications not discussed to any large extent here would become amenable to study as well. Medical applications, such as angiography, can be tested for feasibility. Investigations of the structure of organic molecules via x-ray diffraction would become much more efficient. X-ray fluorescence could be applied to trace-element analysis. We

include, as an appendix to this proposal, a paper presented at a recent SPIE conference on these subjects.<sup>41</sup> In addition, a host of potential applications to materials studies would become available for laboratory testing, notably those involving superlattices and crystals encompassing impurity domains, such as oxygen (or nitrogen) platelets. These latter might have important applications, for example, to semiconductor technology.

The list goes on. We are excited by the future prospects of the field. A CEBAF-injector beam line would make them possible.

## REFERENCES

1. R.L. Walker *et al.*, Phys. Rev. Lett. **25**, 5 (1970); R.L. Walker, B.L. Berman, and S.D. Bloom, Phys. Rev. A **11**, 736 (1975).
2. M.A. Kumakhov, Phys. Lett. **57**, 17 (1976); R.W. Terhune and R.H. Pantell, Appl. Phys. Lett. **30**, 265 (1977).
3. M.J. Alguard *et al.*, Phys. Rev. Lett. **42**, 1148 (1979); R.L. Swent *et al.*, Phys. Rev. Lett. **43**, 1723 (1979).
4. M. Gouanère *et al.*, Nucl. Instrum. Methods **194**, 225 (1982) and Phys. Rev. B **38**, 4352 (1988).
5. B.N. Kalinin *et al.*, Phys. Lett. **70A**, 447 (1979), S.A. Vorobiev *et al.*, Sov. Phys. J. **21**, 1483 (1979), JETP Lett. **29**, 375 (1979), and JETP Lett. **32**, 241 (1980), and Yu.N. Adishchev *et al.*, JETP Lett. **30**, 402 (1979), Phys. Lett. **83A**, 337 (1981), and JETP Lett. **33**, 462 (1981); A.O. Agan'yants *et al.*, JETP Lett. **29**, 505 (1979); I.I. Miroshnichenko *et al.*, JETP Lett. **29**, 722 (1979); V.I. Vit'ko *et al.*, Sov. Phys.--Tech. Phys. Lett. **5**, 541 (1975) and V.B. Ganenko *et al.*, JETP Lett. **32**, 373 (1980) and Radiation Effects **62**, 167 (1982); N.A. Filatova *et al.*, Phys. Rev. Lett. **48**, 488 (1982) and Nucl. Instrum. Methods **194**, 239 (1982); M. Atkinson *et al.*, Phys. Lett. **110B**, 162 (1982) and J.F. Bak *et al.*, Proc. Int. Conf. Atomic Collisions in Solids (1983), pp. 48 and 144.
6. N. Cue *et al.*, Phys. Lett. **80A**, 26 (1980) and Nucl. Instrum. Methods **230**, 104 (1984); J.E. Watson and J.S. Koehler, Phys. Rev. A **24**, 861 (1981) and Phys. Rev. B **25**, 3079 (1982); J.U. Andersen and E. Laegsgaard, Phys. Rev. Lett. **44**, 1079 (1980), J.U. Andersen, K.R. Eriksen, and E. Laegsgaard, Phys. Scr. **24**, 588 (1981), J.U. Andersen *et al.*, Phys. Rev. Lett. **49**, 215 (1982) and Nucl. Instrum. Methods **194**, 209 (1982), and J.U. Andersen, E. Laegsgaard, and A.H. Sorensen, Nucl. Instrum. Methods **230**, 63 (1984).
7. Most of the results from approximately 50 papers reporting channeling-radiation experiments performed at Livermore up to 1986 have been reviewed in one or another of the following: B.L. Berman and S.D. Bloom, Energy Tech. Rev. **81-1**, 1 (1981); B.L. Berman and S. Datz, in *Coherent Radiation Sources* (eds. A.W. Saenz and H. Überall, Springer, Berlin and Heidelberg, 1985), Ch. 7, p. 165; B.L. Berman *et al.*, Nucl. Instrum. Methods **B10/11**, 611 (1985); B.L. Berman, Energy Tech. Rev. **85-3**, 12 (1985); B.L. Berman *et al.*, in *Relativistic Channeling* (eds. R.A. Carrigan, Jr. and J.A. Ellison, Plenum, New York, 1987), p. 239; R.H. Pantell *et al.*, *ibid.*, p. 435; and B.L. Berman, Radiation Effects and Defects in Solids **122-123**, 277 (1991).

8. M.A. Kumakhov and R. Wedell, *Radiation of Relativistic Light Particles during Interaction with Single Crystals* (Spektrum, Heidelberg, 1991; with 303 references).
9. W. Lotz *et al.*, Nucl. Instrum. Methods **B48**, 256 (1990).
10. W.J. Beezhold *et al.*, Bull. Am. Phys. Soc. **30**, 374 (1985) and to be submitted for publication.
11. R.K. Klein *et al.*, to be submitted for publication; see B.L. Berman, Radiation Effects and Defects in Solids **122-123**, 277 (1991).
12. J.U. Andersen *et al.*, Phys. Rev. Lett. **49**, 215 (1982).
13. J.O. Kephart *et al.*, Phys. Rev. B **40**, 4249 (1989).
14. J.U. Andersen, E. Laegsgaard, and A.H. Sorensen, Nucl. Instrum. Methods **230**, 63 (1984).
15. H. Überall, Phys. Rev. **103**, 1055 (1956); G. Diambri Palazzi, Rev. Mod. Phys. **40**, 611 (1968); U. Timm, Fortschr. Phys. **17**, 765 (1969).
16. M.A. Kumakhov, Phys. Lett. **57A**, 17 (1976); V.V. Beloshitsky and M.A. Kumakhov, in *Coherent Radiation Sources* (eds. A.W. Saenz and H. Überall, Springer, Berlin and Heidelberg, 1985), Ch. 5, p. 91.
17. J.U. Andersen, E. Bonderup, and E. Laegsgaard, Channeling Radiation--Quantum Theory, *ibid.*, Ch. 6, p. 127.
18. S.E. Sandström and H. Überall, Phys. Rev. A **43**, 12701 (1991).
19. J.U. Andersen, K.R. Eriksen, and E. Laegsgaard, Phys. Scr. **24**, 588 (1981).
20. A.W. Saenz, H. Überall, and A. Nagl, Nucl. Phys. **A373**, 90 (1981).
21. P.A. Doyle and P.S. Turner, Acta Cryst. **A24**, 390 (1968).
22. H.A. Bethe, Ann. der Physik **87**, 55 (1928).
23. P.B. Hirsch *et al.*, *Electron Microscopy of Thin Crystals* (Butterworth, London, 1965).
24. G. Kurizki and J.K. McIver, Phys. Rev. **B32**, 4358 (1985).
25. G. Kurizki, Phys. Rev. **B33**, 49 (1986).

26. H. Überall *et al.*, in *Essays in Classical and Quantum Dynamics* (eds. J.A. Ellison and H. Überall, Gordon and Breach, New York, 1991), p. 189.
27. A.W. Saenz and H. Überall, in *Coherent Radiation Sources* (eds. A.W. Saenz and H. Überall, Springer, Berlin and Heidelberg, 1985), Ch.1, p. 5.
28. J.U. Andersen *et al.*, Nucl. Instrum. Methods **194**, 209 (1982).
29. J.U. Andersen *et al.*, Phys. Scr. **28**, 308 (1983).
30. "Etching ICs with X-rays," IEEE Spectrum **14**, No. 9 (1990).
31. A.W. Neureuther, in *Synchrotron Radiation Research*, (eds. H. Winick and S. Doniach, Plenum, New York, 1980).
32. J. Maldonado, private communication (1992).
33. M.A. Piestrup *et al.*, *SPIE 773--Electron-Beam, X-ray, and Ion-Beam Lithographies VI*, (1987), p. 37.
34. R. Hollman, J. Vac. Sci. Technol. **36**, 186 (1988).
35. R. Wedell, Phys. Stat. Sol. (b) **99**, 11 (1980).
36. P. Sprangle, B. Hafizi, and F. Mako, Appl. Phys. Lett. **55**, 2559 (1989).
37. A.D. Wilson, Solid State Tech. **29**, 249 (1986).
38. M.A. Kumakhov, Nucl. Instrum. Methods **B48**, 283 (1990).
39. R. Deslattes in *X Rays from Relativistic Electrons in Periodic Media* (1988).
40. J.O. Kephart, Ph.D. thesis, Stanford University (1987).
41. H. Uberall, B.J. Faraday, X.K. Maruyama, and B.L. Berman, Proc. SPIE Symp. on Optical Applied Science and Engineering, SPIE **1552**, 198 (1991).

**APPENDIX**

**PROCEEDINGS**

 SPIE—The International Society for Optical Engineering

# **Short-Wavelength Radiation Sources**

**Phillip Sprangle**  
*Chair/Editor*

**24-25 July 1991**  
**San Diego, California**



**Volume 1552**

# Channeling radiation as an x-ray source for angiography, x-ray lithography, molecular structure determination, and elemental analysis

H. Überall\* and B.J. Faraday

SFA, Inc., 1401 McCormick Drive, Landover, MD 20785

X.K. Maruyama

Department of Physics, Naval Postgraduate School  
Monterey, CA 93943

B.L. Berman

Department of Physics, George Washington University  
Washington, DC 20052, USA

## ABSTRACT

Synchrotron radiation of 33 keV ( $\lambda \approx 0.4 \text{ \AA}$ ) has been tentatively employed for coronary angiography studies; the results were successful, but so far lack clinical quality. Synchrotron radiation has also been proposed as a source for microlithography and the efficient production of integrated circuits, using energies of 0.5 - 2.5 keV ( $\lambda \approx 5\text{-}20 \text{ \AA}$ ). This application, although not yet carried out in earnest, appeared promising enough so that a number of synchrotron sources dedicated to this purpose are now being set up worldwide. Such applications require storage rings for GeV electrons, costing \$20 to 60 million each. Less expensive, lower energy linacs, affordable by individual hospitals or smaller institutions, can produce keV channeling radiation suitable for microlithography and angiography. Channeling-radiation intensities, especially for x-ray energies of some tens of keV and higher will surpass synchrotron-radiation intensities. We have carried out quantitative studies confirming the above conclusions regarding the comparison of channeling radiation and synchrotron radiation. We found that  $< 5\text{ MeV}$  electron linacs costing less than \$1 million can generate few-keV channeling radiation intensities comparable to that of synchrotron radiation, suitable for microlithography and calcium-based angiography, as well as x-ray diffraction structure analysis and elemental analysis by x-ray fluorescence. (For iodine-based angiography, 20 MeV linacs are required.) If transition radiation were used for the same purposes, more expensive linacs of an order of magnitude higher electron energy would be needed.

## 1. CHANNELING RADIATION IN PERSPECTIVE

x-rays are obtained from the impact of electrons on matter. If the matter is amorphous, bremsstrahlung is emitted (we may call it incoherent bremsstrahlung or IB). If the electrons impact on crystalline targets, they can produce coherent bremsstrahlung (CB), channeling radiation (CR),

---

\*Also at the Naval Research Laboratory, Code 4694, Washington, DC 20375 and Department of Physics, Catholic University of America, Washington, DC 20064.

or parametric x-rays (PX), with descending values of the frequency of radiation. If the electrons impact on foil targets, they generate transition radiation (TR). Synchrotron radiation (SR) is produced if the electrons circle around a synchrotron or a storage ring.

Kumakhov has stated<sup>1,2</sup> (see also Pantell<sup>3</sup>) that channeling radiation of electrons in monocrystals constitutes the most intense known radiation source for soft or hard x-rays. If diamond targets are used, a 20-MeV electron linac (available for approximately \$1 million) can produce intense, monochromatic, and polarized x-rays up to the 30-keV range<sup>4</sup> in a tunable fashion, suitable for iodine-based angiography. Less expensive, lower energy linacs, e.g., the Varian linatron (affordable by smaller institutions, individual hospitals, and companies) which can produce few-keV channeling radiation<sup>5</sup>, are suitable for microlithography, elemental analysis by x-ray fluorescence, x-ray diffraction structure analysis of macromolecules and crystals, and also for calcium-based angiography. Channeling radiation intensities are comparable to that of synchrotron radiation, and depending on the choice of target crystals (tungsten or silicon, rather than diamond) will surpass it especially for x-ray energies of some tens of keV and up.<sup>4,6,7</sup>

CR is produced in the form of near-monochromatic spikes<sup>4,6</sup> (which incidentally are also highly linearly polarized<sup>8</sup>.) For all application discussed below, except for x-ray lithography, monochromaticity is required. If IB or SR (which have a broad spectrum) were used for these, it would first have to be monochromatized, with a corresponding large loss in intensity (several orders of magnitude.)

Figure 1 shows schematically the spectrum of photons generated by 10-MeV electrons. Incoherent bremsstrahlung provides a smooth spectrum up to the electron energy. However, the intensity is low. Coherent bremsstrahlung appears at higher energies, giving relatively monoenergetic photons. There are two types: type B provides MeV photons, and type A provides more intense photons of 100 keV. Channeling radiation provides 10 keV photons. Transition radiation (TR) is below the keV region, and parametric x-rays (PX) are at still lower energy. TR is shown as a (broad) peak because the self-absorption of the x-rays in the foil stack eliminates the soft x-rays. Parametric x-rays may be viewed as the Bragg reflection of virtual photons accompanying the electron, and becoming real photons in the process.

The critical requirement for channeling is the angular divergence of the electron beam. The electrons oriented within the Lindhard critical angle

$$\Psi = (Ze^2/Ed)^{1/2} \approx \gamma^{-1/2} \quad (1)$$

where  $d$  is the crystal periodicity, will be channeled. An important feature to note is that the energy dependence is in the denominator. This means that for lower energies, the beam quality requirements are less. For 10 MeV, the Lindhard angle is a few mrad, which is about what is achievable for available commercial accelerators.

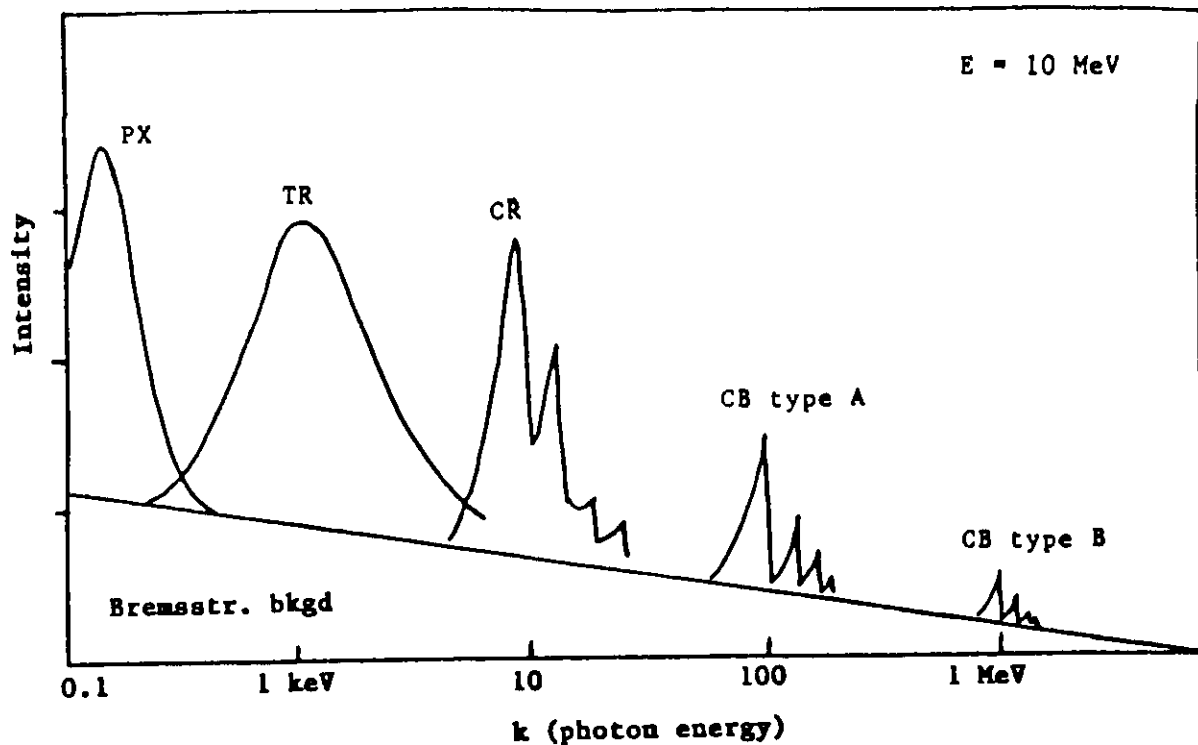


Figure 1. X-ray generation by 10 MeV electrons

PX = parametric X-rays  
 TR = transition radiation

CR = channeling radiation  
 CB = coherent bremsstrahlung

Another advantage for considering channeling radiation is the low energy requirement. The advantages include not only the lower cost for the accelerator and facility, but personnel safety. Shielding requirements are much less and shielding against neutrons no longer is an issue. The separation energies of neutrons are greater than 7 MeV in most cases, and greater than 10 MeV for most light nuclei. This implies that activation need not be a significant inhibiting factor.

The question at hand is whether there is sufficient intensity to make channeling radiation interesting. Integrating Andersen's<sup>5</sup> formula for the number of photons  $N$  per unit solid angle per unit length of crystal (which also shows that the opening angle of the emitted CR cone is  $\theta \approx 1/\gamma$ ,  $\gamma = E/m$  being the Lorentz factor of the electrons) leads to the scaling law

$$\frac{dN}{dz} \propto \gamma^4 \quad (2)$$

so there is a trade-off between higher intensity and lower energy. This relationship allows us to scale expected results from existing data.

Lotz et al<sup>9</sup> have recently carried out an extremely important experiment on CR. Using the superconducting linac at Darmstadt, they observed x-rays from diamond and silicon using electron energies of 4-7 MeV; ~5keV x-rays were observed from axial channeling. Their beam divergence was 0.05 mrad, which is two orders of magnitude better than the Lindhard angle. This means that